Title
Combination Therapy to Enhance Cancer Treatment

Author
Guo, Yiping

Publication Date
2020

Peer reviewed|Thesis/dissertation

UNIVERSITY OF CALIFORNIA, MERCED

Combination Therapy to Enhance Cancer Treatment

A dissertation submitted in partial fulfillment of the requirements for the degree of Doctor of Philosophy

in

Quantitative and Systems Biology

by

Yiping Guo

Committee in Charge:

Professor Wei-Chun Chin, Chair
Professor Changqing Li, Supervisor
Professor Chih-Chun Chien
Professor Joel Spencer

2020

The dissertation of Yiping Guo is approved, and it is acceptable in quality and form for publication on microfilm or electronically:

Professor Wei-Chun Chin

Professor Changqing Li

Professor Chih-Chun Chien

Professor Joel Spencer

University of California, Merced

2020

Dedication

To my parents, grandparents and other family members. Thanks for your support along the journey of earning Ph.D. degree.

I dedicated this thesis to my beautiful hometown Chengdu, Sichuan (Szechuan), where my soul belongs to.

Table of Contents

List of Figures

ACKNOWLEDGEMENTS

Firstly, I would like to thank my advisor, Dr. Changqing Li for the support during my graduate study in Biomedical Imaging Lab, UC Merced. Dr. Li is very knowledgeable, supportive and providing me with lots of great ideas and advice. I have learned a lot from him on how to stay motivated and how to become a professional researcher.

Next, I would like to thank my committee members, Dr. Wei-Chun Chin, Dr. Chih-Chun Chien and Dr. Joel Spencer who provided me great suggestions during the committee member meetings and I highly appreciate their time and effort for serving as my committee members.

Then, I would like to show my appreciation for the members and alumni in the Biomedical Imaging Lab: Wei Zhang, Yue Zhang, Michael Lun, Ignacio Romero, Yile Fang, Yibing Zhang, Jarrod Cortez, and Steven Soe. Our lab has a great atmosphere to work and to stay with. I'm so grateful for the time to spend with such nice people.

I am grateful for the colleagues whom I worked with throughout my Ph.D. study: Dr. Shih-Ming Tsai, who has helped me getting familiar with the lab set up. Dr. Roy Hoglund and Emily Slocum from the Department of Animal Research Service, who helped me operating Gamma irradiator. Hongmei Liu, Yushi Liu, Juanru Liu and Minghao Yuan, whom I worked with for the combination cancer therapy projects.

I would like to thank Rimei Chen, Haoling Liang, Ting Liu, Lu Yi, Shaozhuan Li, Shangjie Ma, and Wenyan Guan who have shown friendships and great support during the COVID-19 pandemic.

Finally, I would like to thank my parents for the love and support. I'm proud to be the second Dr. Guo in the family and I'm lucky to have such wonderful parents who are willing to listen and understand all my choices. I would like to thank my family members Xiaogu Wen, Hongchou Chen, Xi Chen, Zongjing Chen and Wei Gan, who have always been by my side and love me unconditionally.

CURRICULUM VITAE

Education

2015- 2020 PhD in School of Natural Sciences, Quantitative Systems Biology program

- Supervised by Professor Changqing Li
- Photodynamic Therapy for Cancer
- Nanoparticle Synthesis and Drug Delivery

2013-2015 MSc in School of Medical Sciences, University of Macau

- Supervised by Chair Professor Yitao Wang
- Drug Design
- Natural Products and Biosynthesis

2009-2013 BSc in School of Pharmacy, Chengdu University of TCM

- Pharmaceutical Chemistry
- Synthetic Chemistry

Patent

L. Guo, L. Xiong, T. Zhang, X. Li, P. Guo, **Y. Guo** and Y. Han. Granted in 2017 'A Lignan glycoside compounds and its preparation methods.'
CN104151373B/WO2014183630A1 (PCT)

Publication

1. **Y. Guo[1]***, H. Liu[1]*, H. Xiao[1]*, M. Yuan, Y. Liu, V. Sedlarik, W-C. Chin, J. Liu, L. Guo and C. Li. 2020 Curcuminoids Conjugate for Combinational Chemo-Photodynamic Cancer Therapy. 2020 Journal of Photochemistry & Photobiology, B: Biology *Under review*
2. **Y. Guo**, S. Sheng, M. Lun, S. Tsai, W. Chin, R. Hoglund and C. Li 2020 Photodynamic Therapy Excited by Cerenkov Radiation from Cesium-137

Irradiator: In vitro Studies. Clinical Oncology and Research 3:6 (2020) 2-5 http://dx.doi.org/10.31487/j.COR.2020.06.07

3. H. Xiao[1]*, **Y. Guo[1]***, H. Liu, Y. Liu, Y. Wang, C. Li, J. Cisar, D. Skoda, I Kuritka, L. Guo and V. Sedlarik 2019 'Structure-based Design of Charge-conversional Drug Self-delivery System for Better Targeted Cancer Therapy' Biomaterials 232 (2020)119701 https://doi.org/10.1016/j.biomaterials.2019.119701
4. **Y. Guo**, S. Sheng, W. Zhang, M. Lun, S. Tsai, W. Chin, R. Hoglund and C. Li. 2018 'High Energy Photons Excited Photodynamic Cancer Therapy in vitro' SPIE BiOS Proceeding,104760T (2018) https://doi.org/10.1117/12.2291252
5. W. Zhang, **Y. Guo**, C. Li 2016 'X-ray Luminescence Computed Tomography: an emerging molecular imaging modality' Instrumentation 04 (2016) CNKI
6. **Y. Guo**, L. Lin and Y. Wang 2015 'Chemistry and pharmacology of the herb pair Flos Lonicerae japonicae-Forsythiae fructus' Chinese Medcine 10:16 (2015) doi: 10.1186/s13020-015-0044-y
7. C. He, C Peng, X. Xie, L. Guo, Q. Zhou, X. Li, O. Dai, Z. Geng and **Y. Guo** 2013 'Two New Dianthramide Glucosides with Cardiomyocytes Protective Activity from Aconitum Carmichaelii' Phytochemistry Letters 6:2 (2013) 299-301. https://doi.org/10.1016/j.phytol.2013.03.008
8. L. Guo, C. Peng, O. Dai, Z. Geng, **Y. Guo**, X. Xie, C. He and X. Li 2013 'Two New Pyrazines from the Root of Aconitum Carmichaelii' Biochemical Systematics and Ecology 48 (2013) 92-95 https://doi.org/10.1016/j.bse.2012.12.009
9. Q. Ye, **Y Guo** and C. Peng 2013 'The impact on alkaloids constituents of Aconiti lateralis Radix in different processing methods' West China J of Pharma. Sci. 28:3 (2013) 275- 277 CNKI
10. Q. Ye, **Y. Guo**, C. Peng and L. Guo 2013 "Component research about Aconiti lateralis Radix prepapata compatible with fresh ginger, dried ginger, sand-fried ginger" Chinese Traditional Patent Medicine 35:5 (2013) 1035-1039 CNKI

Presentation and Poster

1. Y. Guo 2019 'A Self-Delivery Drug System for Cancer Therapy' 20th Annual

University of California System-wide Bioengineering Symposium

2. Y. Guo 2018 'In vitro Studies of High Energy Photons Excited Photodynamic Cancer Therapy' 19th Annual University of California System-wide Bioengineering Symposium
3. Y. Guo 2018 'In vitro Studies of High Energy Photons Excited Photodynamic Cancer Therapy' SPIE BiOS, Optical Methods for Tumor Treatment and Detection: Mechanisms and Techniques in Photodynamic Therapy
4. Y. Guo 2015 'Chemistry and pharmacology of the herb pairs" 28th International Symposium on the Chemistry of Natural Products

---

Teaching Experience

2015-2016: Teaching Assistant of 'CHEM02 General Chemistry I - UC Merced

2017: Teaching Assistant of 'CHEM10 General Chemistry II - UC Merced

2018-2019: Teaching Assistant of 'BIO02 Introduction to Molecular Biology - UC Merced

2019-2020: BIO02 Introduction to Biology Discussion - UC Merced

---

Scholarships and Honors

2020 April QSB Dissertation Incentive Award University of California, Merced, USA

2017-2020: School of Natural Sciences summer research fellowship UC Merced, USA

2013-2015: Research Fellowship, University of Macau, Macao SAR

Abstract of the Dissertation

Combination Therapy to Enhance Cancer Treatment

by

Yiping Guo

Doctor of Philosophy, Quantitative and Systems Biology
University of California, Merced, 2020

Ph.D. Advisor: **Professor Changqing Li**

Cancer is the second leading cause of death worldwide. Surgery, chemotherapy, radiotherapy, and photodynamic therapy are widely used treatment modalities for cancer. However, the toxicities of cancer treatments and the tendency to induce drug resistance cause limitations to combat this disease with mono-therapeutic approaches. To address this issue, combination therapy, a treatment modality that combines more than one therapeutics, has been introduced to improve the current treatments based on a synergistic outcome. This approach can potentially reduce serious side effects, while providing the enhancement to therapeutic efficacy. In this dissertation, I performed different modules of combinatorial cancer therapy methods to verify the enhancement of anti-tumor efficacy both in vitro and in vivo. Chapter 1 provided the introductory research background as well as current challenges in cancer therapeutic methods. In Chapter 2, I present the study that photodynamic therapy efficacy was excited by the Cerenkov Radiation from Cesium-137 irradiator. In Chapter 3, I outlined the findings of multiple anti-cancer agents: camptothecin derivative and curcuminoids assembled into nanoparticles, and these nanoparticles exhibit better tumor targeting and eliminate the severe side effects caused by camptothecin derivatives. In Chapter 4, I applied a combination of the chemotherapy anti-cancer agents with photodynamic therapy to achieve the enhancement of anti-tumor efficacy both *in vitro* and *in vivo*. And finally, in Chapter 5, I concluded that the combination therapy compared to the monotherapy will achieve better anti-tumor performance. Altogether, our data showed that compared to the monotherapy, the combination therapy will achieve better anti-cancer performance. These results provide new opportunities to develop better cancer therapy methods.

CHAPTER 1

INTRODUCTION OF COMBINATION THERAPY FOR CANCER

1.1 Introduction

Cancer is the second leading cause of death in the United States, exceeded only by heart diseases. One of every four deaths in the United States is due to cancer. As an extremely fatal disease, about 1 in every 6 deaths is due to cancer. [1] Despite the increasing cancer mortality, new types of anti-cancer agents contribute very little to make improvement mainly caused by the financial burden for designing those agents. The development of new types of anti-cancer agents in laboratories is expensive. The initial process required a huge amount of pre-clinical experimental studies, and the subsequent clinical trials before getting the approval from FDA. [2,3] So, it is important to explore more efficient approaches to utilize the traditional anti-cancer methods in order to design enhanced forms of therapeutics which are also feasible in economics. [4] Another long-term challenge for cancer therapy is drug resistance. Multiple regulatory cell signaling pathways have been found defectively to compromise their treatment efficacy during the process of tumor generation including cell cycle arrest, apoptosis, or migration. Such cellular heterogeneity in cancer cells might cause limitations to combat this disease with mono-therapeutic approaches [5]. In aim to address this issue, the combination therapy with the ability to suppress more than one pathway has reported improving the current treatments based on a synergistic therapeutic outcome [6,7,8]. The combination therapy strategy has already been utilized in the clinic, known as drug cocktail therapy. Studies have found that multi-pronged assault to tumors through administering a cocktail of different anti-cancer agents could achieve synergistic anti-tumor efficacy, improve tumor targeting selectivity, deter the drug resistance, and minimize the severe side effects compared to the respective mono-therapeutics. [9,10]

1.2 Origin of Cancer Cells

As tissues in the process to grow and renew themselves, each individual cell must adjust its behavior to surroundings as the needs of the organism as a whole. The cells have to divide to the type of cells that are needed, maintain their specialized characters, and occupy the proper places. And cells must ingest nutrient fuels such as carbohydrates, lipids, and amnio acids from the surroundings to generate energy. In large organisms, occasional cell misbehaves, and random mutations cause no significant harm. But potentially changes of the environment or the lack of nutrition supply will cause cells suffer genetic alteration that

that behave in the same way of manners. With such dysfunctional behaviors, cells can disrupt the organization of the tissue, and eventually expand to whole body system. [11]

A tumor is cancerous only if its cells have the ability to invade surrounding tissue, in this case, the tumor is said to be malignant. Malignant tumor cells with invasive property can enter the bloodstream or lymphatic vessels, where they will form the secondary tumors at other sites in the body. Environmental changes like irradiation, hypoxia and inflammation are the factors to induce cancer cell formation. Epidemiology research reveals other factors that increase the risk of cancer. Obesity, smoking, drinking and exposure of sun rays might also raise the incidence of several cancers. [11] Although environmental factors affect the incidence of cancer and are critical for some forms of the disease, it would be wrong to conclude that they are the only cause of cancers. No matter how hard we try to prevent cancer by healthy living, we might never be able to eradicate this disease. To devise effective treatments, we need to derive a deep understanding of the biology of cancer cells and the mechanisms that underlie the growth and spread of tumors. [12]

1.3 Types of Cancer Treatment

Surgery, radiation, chemotherapy and photodynamic therapy are well established cancer treatments, but many new approaches have also been pursued in recent studies. Sometime, with loss of a normal response to DNA damage, the distinct feature that makes the cancer cell harmful and dangerous can also make it vulnerable, enabling researchers and doctors find out a way to kill it with targeted cancer treatments. For example, some types of breast cancers owe their genetic instability to the lack of a protein (namely Brca1 or Brca2) needed for accurate repair of double-strand breaks (DSBs) in DNA. The cancer cells survive by relying on alternative types of DNA repair mechanisms. Drugs that inhibit one of these alternative DNA repair mechanisms kill the cancer cells by raising their genetic instability, leading to chromosome fragmentation. Normal cells, however, with validate double-strand break repair mechanism, are unaffected at this point. [13] Another set of strategies aims to use the human immune system to kill the tumor cells, taking advantage of tumor-specific surface molecules to target the attack. Antibodies that recognize these tumor-specific molecules can be produced *in vitro* and injected into patients to target the tumor cells for destruction. Other antibodies, aimed at the immune cells, can promote the elimination of cancer cells by neutralizing the inhibitory cell-surface molecules. [14]

The task is made more challenging because the mutations arise randomly, every case of cancer is likely to have its own unique combination of genes mutated. Even within an individual patient, tumor cells do not all contain the same genetic lesions. Thus, no single treatment is likely to work in every patient, or even for every cancer cell within the same patient. [15]

1.4 Combination Therapy for Cancer

Combination therapy was first reported in 1965 by Emil Frei, James F. Holland and Emil J. Freireich for the proposed research using combination chemotherapy for acute leukemia [16]. Pediatric patients who diagnosed with acute lymphocytic leukemia were treated with the combination of methotrexate, 6-mercaptopurine, vincristine and prednisone (formally known as the POMP regimen) and was proven successful in reducing tumor growth and prolonging remission of prostate cancer [16]. As the consequence, research in cancer therapy became focused on exploring and designing combination therapies that target different pathways to create a synergistic effect. In addition, researchers have found that combination displayed selective toxicity and a reduction in tumor growth rate *in vitro* and *in vivo* on pancreatic ductal adenocarcinoma [17,18]. Thus, using a combination of compounds that target different pathways, a synergistic or potentiation effect could yield remarkable anti-cancer outcomes.

The combination of more than one therapeutic treatment to specifically target cancer-inducing or cell-sustaining pathways is a cornerstone of cancer therapy [19]. Although the mono-therapy approach is still a very common treatment modality for many cases of cancer, this conventional method is less effective in many ways than the combination therapy approach does [20]. Conventional mono-therapeutic techniques with non-selective targets ultimately lead to the destruction of the whole-body system, including healthy cells. Chemotherapy can be very cytotoxic to the patient with multiple severe side effects and can also weaken their immune system by affecting bone marrow's ability and increasing vulnerability [17, 18]. Although combination therapy can be cytotoxic as one of the chemical agents used for chemotherapy, the toxicity is reduced because of different pathways targeted. And because combination therapy works in a synergistic manner, and therefore administration dosage of each drug required would be low. Additionally, combination therapy may be able to reduce side effects on normal cells while simultaneously producing cytotoxic effects on cancer cells. [19, 20].

Another therapeutic approach that has gained publicity in cancer research is repositioning of current drugs. It is a therapeutic approach where current pharmaceutical agents primarily used for non-cancerous diseases are now being used for cancer treatment [21]. This approach is efficient because the aimed drugs have already passed drug safety protocols and have known pharmacokinetic profiles [22]. One such example would be acetazolamide, (AZ), a pan-carbonic anhydrase inhibitor. AZ is typically used for the treatment of glaucoma and altitude sickness but has now been proposed for the treatment of cancer [23, 24]. Researchers discovered that cancer cells display high carbonic anhydrase activity, which correlates with malignant behavior. And therefore, inhibiting this activity would create anti-cancer effects. Repositioning drugs would be also useful when traditional anti-cancer monotherapy has failed to provide a safe and painless treatment for cancer patients [25]. In this way, repositioning and reusing of drugs have provided cancer research with new opportunities with efficiency and efficacy, while also reducing the financial burden associated with drug design and discovery.

1.5 Pathways Involved in Tumor Growth and Targeted Cancer Therapies

In this section, some important cellular pathways in cancer will be discussed. These pathways involved in the tumor growth and sustainment include hypoxia, antioxidant response, and apoptosis. Because of the strong implication in cancer research, the studies in Chapter 3 and Chapter 4 will further illustrate their roles in tumor growth and cancer therapies.

1.5.1 Hypoxia Pathways

Cancer cells have many properties that are different from normal cells, and one of those important properties is their abnormal growing microenvironment due to the vascular abnormalities. This abnormal growth of pattern consequently results in large gaps of diffusion in between blood vessels and veins [26, 27]. Lacking oxygenated blood supply, the tumor will then create strong hypoxic conditions favoring toward the initiation of cancer cells. The lack of oxygen inhibits tumor differentiation and allows the maintenance of cancer stem cells [28]. Additionally, hypoxic conditions will drive cancer cells toward anaerobic glycolysis, instead of oxidative phosphorylation, which consequently leads to lactic acid accumulation and results in a lower extracellular pH level in the tumor microenvironment [29]. During hypoxia, hypoxic inducible factor-1 (HIF-1alpha) translocate into the nucleus, where it dimerizes with HIF-1beta and leads to the expression of genes that are involved in angiogenesis, epithelial-mesenchymal transition, and cellular survival. One of the most important genes activated by HIF1alpha is carbonic anhydrase (CA) [30]. CAs help tumorous cells adapt to hypoxic stress by converting reversible reactions of carbon dioxide to a proton and bicarbonate and thereby provide alkali to the acidic conditions of the cancerous microenvironment [30, 31].

1.5.2 Antioxidant Response Pathways

Under extreme oxidative stress, cells have developed a pathway to adapt to the stress through an antioxidant response, namely the Nrf2-Keap1 pathway. Once the interaction occurs, Nrf2 was ubiquitinated, targeting it for proteasomal degradation [32, 33]. However, under extreme oxidative stress, either due to the accumulation of carcinogens or the generation of reactive oxygen species (ROS), Nrf2 will then be localized in the cell nucleus to elicit anti-oxidative responses. Nrf2 is also involved in the regulation of drug metabolism, cyto-protection, proliferation, apoptosis, growth, and differentiation. Once Nrf2 translocated to the cell nucleus, Nrf2 will recruit other transcriptional machinery, such as CREB binding protein (CBP), coactivator-associated arginine methyltransferase (CARM1) and protein arginine methyltransferase (PRMT1), leading to transactivation [34]. The elevated levels of Nrf2 have shown enhanced growth potential within the cancer cells and increased drug resistance, thus, it is potential that therapeutic agents that turn down Nrf2

expression would expose cancer cells to intrinsic oxidative stress, leading to induction of programmed cell death.

1.5.3 Apoptosis Pathways

Apoptosis is a specific process that leads to programmed cell death through the activation of intracellular pathways leading to pathogenetic cellular changes which are distinct from cellular necrosis. [35] Cell Apoptosis is involved in the general development of normal tissues. This type of programmed cell death is distinctly different from necrosis, for which involved cellular mechanisms and cell morphology are not the same. The morphologic appearance changes include cell membrane shrinkage, cytoplasm blebbing, the condensation of chromatin and disorder of cell organelles. The mechanism of cell death can characterize through the DNA double strands damage with failure of mitosis and endogenous apoptotic mechanism to induce the programmed death. During tumor growth, inhibition of apoptotic death is complemented by the activation of protective and pro-survival response mechanisms for cancer cell development. Thus, new therapeutic agents based on compounds that are designed to target apoptotic and cell cycle pathways became very challenging and appealing. [36]

References

[1] R.L. Siegel, K.D. Miller, A. Jemal, Cancer statistics, 2019. CA A Cancer J Clin, 69 (2019) 7-34. https://doi.org/10.3322/caac.21551

[2] Garattini S. New approaches to cancer therapy. Ann Oncol, 14 (2003) 813-816.

[3] J. A. DiMasi, R. W. Hansen, H. G. Grabowski. The price of innovation: new estimates of drug development costs. J Health Econ. 22 (2003) 151-185.

[4] M. O. Palumbo, P. Kavan, W. H. Miller, L. Jr. Panasci, S. Assouline, N. Johnson, V. Cohen, F. Patenaude, M. Pollak, R. T. Jagoe, G. Batist, Systemic cancer therapy: achievements and challenges that lie ahead, Front Pharmacol. 4 (2013) 57, https://doi.org/10.3389/fphar.2013.00057

[5] S. H. Chen, G. Lahav, Two is better than one; toward a rational design of combinatorial therapy. Curr. Opin. Struct. Bio. 41 (2016) 145–150. https://doi.org/10.1016/j.sbi.2016.07.020

[6] R. Bayat Mokhtari, T. S. Homayouni, N. Baluch, E. Morgatskaya, S. Kumar, B. Das, H. Yeger, Combination therapy in combating cancer. Oncotarget. 23 (2017) 38022–38043. https://doi.org/10.18632/oncotarget.16723

[7] Y. Wen, W. Zhang, N. Gong, Y. F. Wang, H. B. Guo, W. Guo, P. C. Wang, X. J. Liang, Carrier-free, self-assembled pure drug nanorods composed of 10-hydroxycamptothecin and chlorin e6 for combinatorial chemo-photodynamic antitumor therapy in vivo, Nanoscale 38 (2017) 14347–14356. https://doi.org/10.1039/c7nr03129g

[8] K. Zheng, H. Liu, X. Liu, Y. Wang, L. Li, S. Li, J. Xue, M. Huang, M, Tumor Targeting Chemo- and Photodynamic Therapy Packaged in Albumin for Enhanced Anti-Tumor Efficacy, Int. J. Nanomedicine. 15 (2020) 151–167. https://doi.org/10.2147/IJN.S227144

[9] B. Shrestha, L. Tang, G. Romero, Nanoparticles-Mediated Combination Therapies for Cancer Treatment. Adv. Therap., 2 (2019)1900076. doi:10.1002/adtp.201900076

[10] M. V. Blagosklonny. Analysis of FDA approved anticancer drugs reveals the future of cancer therapy. Cell Cycle, 3 (2004) 1035-1042.

[11] H. Douglas, R. A. Weinberg. Hallmarks of cancer: the next generation. Cell vol. 144 (2011): 646-74.

[12] A. M. Lewandowska *et al*. Environmental risk factors for cancer - review paper. Annals of agricultural and environmental medicine: AAEM 26 (2019): 1-7.

[13] Zugazagoitia, Jon et al. Current Challenges in Cancer Treatment. Clinical therapeutics. 38 (2016) 1551-66.

[14] D. Baxter. Active and passive immunization for cancer.Human vaccines & immunotherapeutics. 10 (2014) 2123-9.

[15] M. R Stratton, *et al.* The cancer genome. Nature 458 (2009) 719-24.

[16] Frei E, Karon M, Levin RH, Freireich EJ, Taylor RJ, Hananian J, Selawry O, Holland JF, Hoogstraten B, Wolman IJ, Abir E, Sawitsky A, Lee S, et al. The effectiveness of combinations of antileukemic agents in inducing and maintaining remission in children with acute leukemia. Blood, 26 (1965) 642-656.

[17] Quinn BA, Dash R, Sarkar S, Azab B, Bhoopathi P, Das SK, Emdad L, Wei J, Pellecchia M, Sarkar D, Fisher PB. Pancreatic Cancer Combination Therapy Using a BH3 Mimetic and a Synthetic Tetracycline. Cancer Res, 75 (2015) 2305-2315.

[18] M. V. Blagosklonny. Targeting the absence" and therapeutic engineering for cancer therapy. Cell Cycle, 7 (2008) 1307-1312.

[19] Partridge AH, Burstein HJ, Winer EP. Side effects of chemotherapy and combined chemohormonal therapy in women with early-stage breast cancer. J Natl Cancer Inst Monogr, 30 (2001) 135-142.

[20] LeBaron S, Zeltzer LK, LeBaron C, Scott SE, Zeltzer PM. Chemotherapy side effects in pediatric oncology patients: drugs, age, and sex as risk factors. Med Pediatr Oncol. 16 (1988) 263-268.

[21] C. R. Chong, D. J. Jr. Sullivan, New uses for old drugs. Nature. 448 (2007) 645-646.

[22] Islam SS, Mokhtari RB, Akbari P, Hatina J, Yeger H, Farhat WA. Simultaneous Targeting of Bladder Tumor Growth, Survival, and Epithelial-to-Mesenchymal Transition with a Novel Therapeutic Combination of Acetazolamide (AZ) and Sulforaphane (SFN). Target Oncol. 11 (2016) 209-227.

[23] M.V. Blagosklonny, Immunosuppressants in cancer prevention and therapy. Oncoimmunology. 2 (2013) 26961.

[24] M.V. Blagosklonny, A new science-business paradigm in anticancer drug development. Trends Biotechnol. 21 (2003) 103-106.

[25] P. Vaupel, L. Harrison L. Tumor hypoxia: causative factors, compensatory mechanisms, and cellular response. Oncologist. 9 (2004) 4-9.

[26] Kim Y, Lin Q, Glazer PM, Yun Z. Hypoxic tumor microenvironment and cancer cell differentiation. Curr Mol Med. 9 (2009) 425-234.

[27] Benej M, Pastorekova S, Pastorek J. Carbonic anhydrase IX: regulation and role in cancer. Subcell Biochem. 75 (2014) 199-219.

[28] Carnero A, Lleonart M. The hypoxic microenvironment: A determinant of cancer stem cell evolution. Bioessays. 38 (2016) 65-74.

[29] Neri D SC. Interfering with pH regulation in tumors as a therapeutic strategy. Nat Rev Drug Discov. 10 (2011) 767- 777.

[30] Svastová E, Hulíková A, Rafajová M, Zat'ovicová M, Gibadulinová A, Casini A, Cecchi A, Scozzafava A, Supuran CT, Pastorek J, Pastoreková S. Hypoxia activates the capacity of tumor-associated carbonic anhydrase IX to acidify extracellular pH. FEBS Lett.577 (2004) 439-445.

[31] Kensler TW, Wakabayashi N, Biswal S. Cell survival responses to environmental stresses via the Keap1-Nrf2- ARE pathway. Annu Rev Pharmacol Toxicol. 47 (2007) 89-116.

[32] Bryan HK, Olayanju A, Goldring CE, Park BK. The Nrf2 cell defence pathway: Keap1-dependent and -independent mechanisms of regulation. Biochem Pharmacol. 85 (2013) 705-17.

[33] Zhang M, A. C, Gao Y, Leak RK, Chen J, Zhang F. Emerging roles of Nrf2 and phase II antioxidant enzymes in neuroprotection. Prog Neurobiol. 100 (2013) 30-47.

[34] Eggler AL, Liu G, Pezzuto JM, van Breemen RB, Mesecar AD. Modifying specific cysteines of the electrophile- sensing human Keap1 protein is insufficient to disrupt binding to the Nrf2 domain Neh2. Proc Natl Acad Sci U S A. 102 (2005) 10070-5.

[35] Bellamy C. 0. C., Malcomson R. D. G., Harrison D. J. and Wyllie A. H. Cell death in health and disease:the biology and regulation of apoptosis.Seminars in Cancer and Biology 6 (1995) 3-16.

[36] Lowe S. W. The role of p53 in apoptosis:In: SluyserM, ed.Apoptosis in Normal Development and Cancer. Taylor & Francis, (1996) 97-126.

CHAPTER 2

PHOTODYNAMIC THERAPY EXCITED BY CERENKOV RADIATION

2.1 Introduction

Cancer is the second leading cause of death in the United States, exceeded only by heart diseases. One of every four deaths in the United States is due to cancer. [1,2] As such, more efforts have been made to improve cancer diagnosis and therapy methods in recent decades. Specifically, chemotherapy and radiotherapy are the primary therapeutic approaches that have been used to treat cancers. However, their drawbacks and side-effects are well-known, including but not limited to extreme pain and discomfort reflected on patients, especially for senior patients. [3,4]

Founded by R. L. Lipson and S. Schwart from Mayo Clinic in 1960s, Photodynamic Therapy (PDT) has become a cancer treatment approach by illuminating dye agents, called photosensitizers, to kill cancer cells. [5,6] The basic principle of PDT is that the excited photosensitizer reacts with oxygen to generate reactive oxygen species (ROS) which are cytotoxic.[7,8] Compared to other therapeutic methods, The photosensitizer is nontoxic until it is excited and the excitation can be selectively delivered to cancerous targets only. Therefore, the side-effects of PDT to normal tissues can be fully controlled and minimized. [9]

A problem with conventional PDT is that the absorption and strong scattering of optical photons from tissues make it difficult to deliver optical photons to deep targets with a typical photon penetration depth of several millimeters, [10,11] which limits the applications of PDT to superficial lesions such as skin cancers or lesions reachable by a light guide. [12,13] Studies have shown that PDT has been applied to treat superficial lesions such as neck cancer, early stage oral cancers, and nasopharyngeal carcinoma. [9] However, to date, there are no reports of applications for deep cancers. To overcome these limitations, high energy photons with high penetration power were introduced to deliver energy for PDT treatment. [13]

Cerenkov radiation is produced when a charged particle travels in a medium with a velocity faster than the speed of light in that medium.[14] Inside tissues, β particles can generate Cerenkov radiation when their energy is larger than 250 keV. [15,16] High energy x-rays or γ-rays can induce highly energetic secondary electrons that can result in Cerenkov radiation for PDT. [17] The high-energy radiation can penetrate deep tissues and deliver the Cerenkov radiation photons to tumors deep inside body. Thus, there are substantial advantages for Cherenkov radiation induced PDT in treating deep tumors. Recent studies

have reported the application of Cerenkov radiation activated PDT using energy mediator titanium dioxide. [18] However, the efficiency of the treatment could be limited due to the administration process. We hypothesized that high energy γ-rays can result in sufficient Cerenkov radiation as the light source for deep tumor target PDT without nanoparticles as energy mediators. Considering that there are plenty of high energy x-ray photons in radiotherapy to induce Cerenkov radiations in tissues and that there are many photosensitizers for clinical applications, we believe the hypothesized approach can be a good complementary cancer therapy for enhancing the efficacy of radiotherapy.

2.2 Methods and Materials

2.2.1 Photosensitizer and Cell Line

The photosensitizer, MPPa ($C_{34}H_{36}N_4O_3$, molecular mass 548.7 gram per mole, 95% purity, Sigma-Aldrich Co. LLC.), was used in this study (Fig. 1). MPPa was first dissolved in acetone (1 mM) and then filtered by 0.2 μm polytetrafluoroethylene syringe filter (Alltech Association Inc., Deerfield, IL). The filtered MPPa was then stored in a dark refrigerator at -20°C. All the following *in vitro* photodynamic therapy experiments were performed on A549 human lung carcinoma cells (Sigma-Aldrich Co. LLC). The cancer cells were cultured using fresh Ham's F12 nutrient mixture medium (L0136, Biowest) supplemented with 100U/mL penicillin and 10% (v/v) Fetal Bovine Serum (FBS, GIBCO) in 5% CO_2.

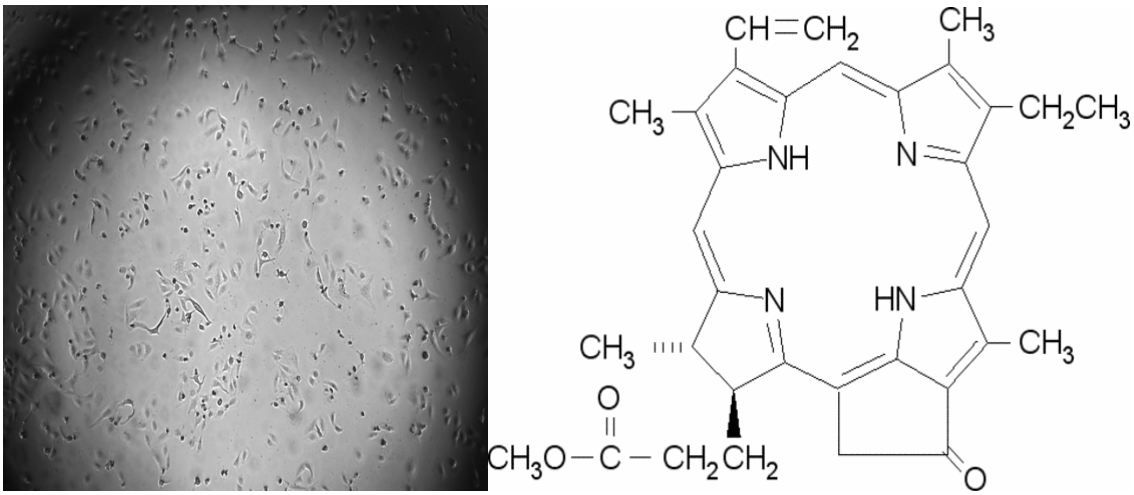

Figure 1. A549 human lung carcinoma cells and photosensitizer: Methyl pyropheophorbide-a (MPPa)

2.2.2 Cesium (Cs)-137 Irradiator Excited PDT

A 2008 manufactured J.L. Shepherd and Associates Mark I-68A 4000Ci Cs-137 irradiator is located at UC Merced Department of Animal Research Service facility as shown in Fig. 2A. The Cs-137 source emits γ-rays with an energy peak of 662 keV. Fig. 2.1 B indicates the three irradiation positions (1, 2, and 3). From the irradiation position and exposure time of samples, we can calculate the radiation dose.

Figure 2. 1. J.L. Shepherd and Associates Mark I-68A 4000Ci Cs-137 irradiator and each irradiator drive shaft position.

2.2.3 Laser Excited PDT

In this study, to validate the efficacy of the photosensitizer, MPPa, we used a pigtailed diode laser (BWF-OEM-650, B&W Tek, 650 nm) with a laser power of 150 mW. As shown in Fig. 2.2 the laser beam was expanded to cover the major part of a cell culture plate with a measured photon density of 4.6±0.05 mW/cm^2.

A549 cells (2.5×10^3 cells per well) were seeded in the wells of each plate. The pre-treated drug solution (1 mM/ ml) was firstly 1:100 diluted. The mixture was then 100%, 50%, 25% and 10% v/v added to cell suspension and the different concentrations of photosensitizer assessment now reads at 10, 5, 2.5, 1 and 0 μM. After rinsing with PBS and fresh F12 medium, the experimental group of plates were irradiated for 7, 15 and 30 minutes respectively. The control group of plates was incubated in dark conditions.

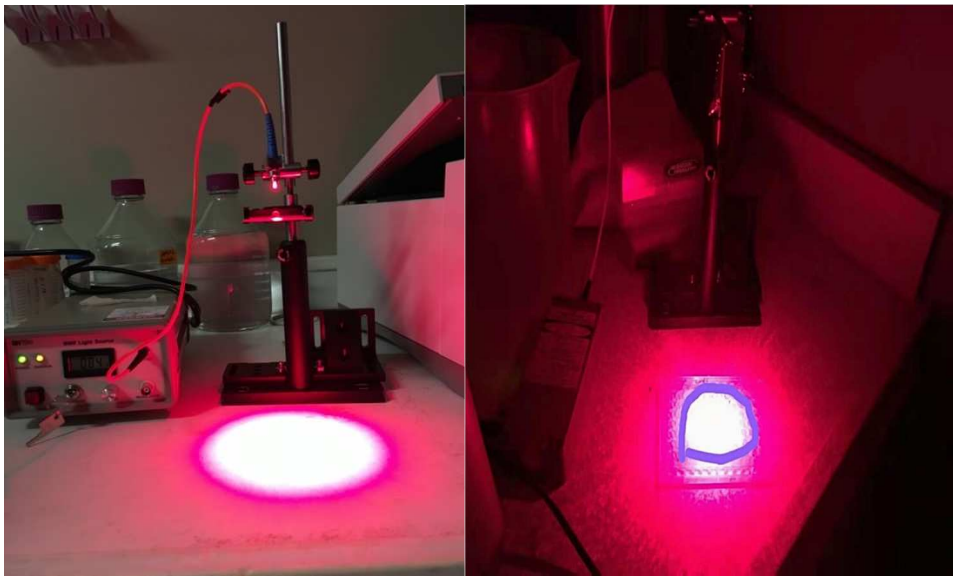

Figure 2. 2 Pigtailed diode laser (BWF-OEM-650, B&W Tek, 650 nm) with a laser power of 150 mW

2.2.4 Cs-137 Irradiator Dose Calibration

A dose rate for each position was first established by measuring the accumulated dose and dividing by the irradiator exposure time then creating a simple linear function to fit our data. The exposure times were ensured to be consistent since the built-in irradiator timer was used (where 1.00 corresponds to 60 secs exposure time). Next, Gafchromic EBT3 films were calibrated with a procedure where the net optical density (NOD) was determined for different doses (determined using the dose rate function). For all films, scanning was performed 3 times each to average the pixel values and reduce noise effects. All film analysis was performed in MATLAB (R2016b, MathWorks) with our own in-house algorithm. Once NOD was determined, the data was plotted as a dose (Gray unit [Gy]) versus NOD plot and the data was fit with a two-term exponential function of the following form:

$$f(x) = a \times \exp(b \times x) + c \times \exp(d \times x)$$

Similar equations were generated for Positions 1 and 2 and then from the equations, the isodose curves can be generated.

2.2.5 High Energy Photons Generated from Cs-137 Irradiator

For this study, a water-based (5% agar) phantom was irradiated under Cs-137(662 keV γ-radiation). Black tape was used as a background test which means no photon penetration. A two-meter fiber bundle was used to capture the potential photons outcomes with one end inside of models and another side connected to spectrograph and EMCCD camera. The whole systems were kept in black box and photon data was real-time recorded and displayed in the oscilloscope.

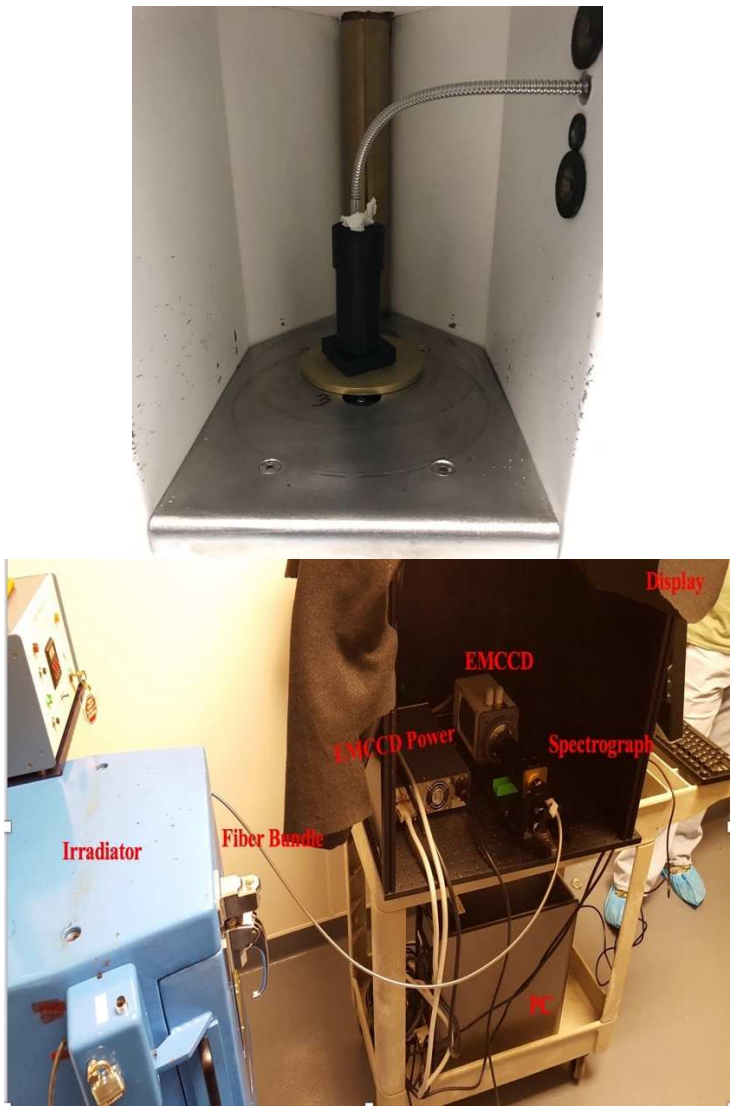

Figure 2. 3 Cs-137 Irradiator with spectrograph and display system

2.2.6 Cell Viability Assay

Photo colorimetric determination of cytotoxicity was assessed using CCK-8 dye (Dojindo Laboratories, Tokyo, Japan) to evaluate cell viability. [19,20] After PDT experiments, cells were incubated in dark for 24 hours and then were washed with PBS buffer. 10% (v/v) CCK-8 assay were added to each well. Then we incubated cells for another 4 hours at 37°C. Finally, the Microplate Reader was used to record optical density (OD) of each well. Using the equation: $(OD_{experimental} - OD_{blank})/ (OD_{control} - OD_{blank})$, we can calculate the cell viability in each well. Then photosensitizers with concentrations of 10 μM, 5 μM, 2.5 μM, 1.0 μM, and 0 μM were added to each column from left to right. The rightmost column, only filled with F-12 medium without cells, was used as background reference (OD_{blank}). For each column, we averaged the measurements from the Microplate Reader (Model number, company) from four wells with a standard deviation.

Eight 96-well plates were divided into four experimental and one control groups, respectively. A549 cells (2.5×10^3 cells per well) were seeded on the plate wells. Then as shown in Fig 2.4, cells in all plates were administered to different concentrations of photosensitizer (0, 1, 2.5, 5, 10 μM). After rinsing with PBS and fresh F12 medium, the four experimental plates were irradiated by the Cs-137 irradiator for 30, 15, 7 and 3 minutes, respectively. Accordingly, the corresponding plates in the control group were placed inside the irradiator for the same times with the radiation source off. Thus, the no radiation group indicates the effects from background light. Cs-137 irradiator delivers γ-rays with an energy peak of 662 keV which is far beyond the threshold of Cerenkov radiation. When using transparent cell plates, the photons could possibly result from plastic scintillation. However, the photons from plastic scintillation inside the black colored plates were absorbed by the black plates thus the plastic scintillation effects on PDT were removed.

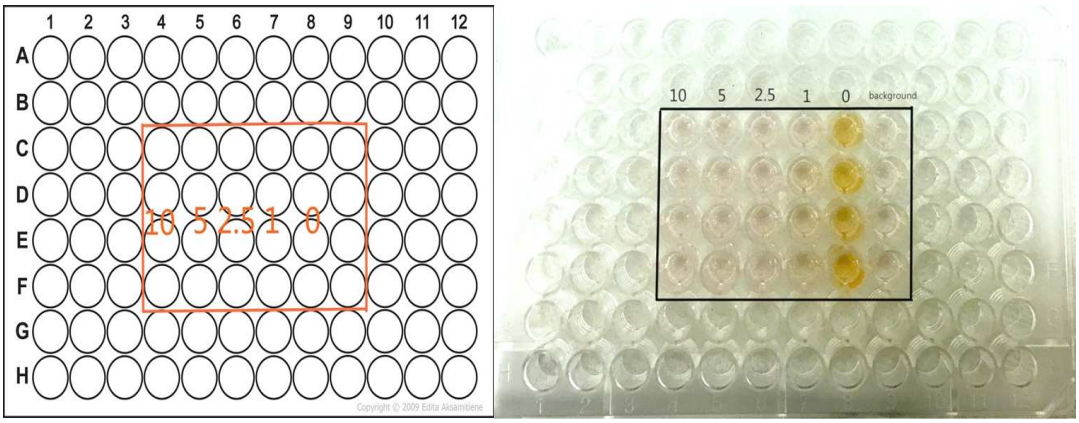

Figure2. 4 MPPa Administration. A549 cells were loaded with different concentrations of photosensitizer. (10, 5, 2.5, 1 and 0 μM)

2.3 Results

2.3.1 Cs-137 Irradiator Dose calibration and Delivered Dose

The resulting isodose curves for each drive shaft position are shown below in Fig. 2.5 A. The cell culture plate was placed at position 3 of the irradiator floor and was stationary during irradiation. Using the generated isodose curve for position 3, the dose rate at the corresponding position is approximately 3.90 Gy/min. With the NOD versus dose function, we created isodose curves for each of the three irradiator drive shaft positions (Fig. 2.5 B). Exposure times for positions 1, 2, and 3 were set to 75s, 90s, and 120s respectively. The Dose (Gy) versus NOD plot for position 3 where a two-term exponential function is fit to our data points is shown in Fig 1B. The resulting exponential function for this position is given by the following

(R^2 = 0.9999, RMSE = 0.03339)

$$\text{Dose (Gy)} = 1.594 * \exp(2.901 * \text{NOD}) - 1.619 * \exp((-0.9637) * \text{NOD})$$

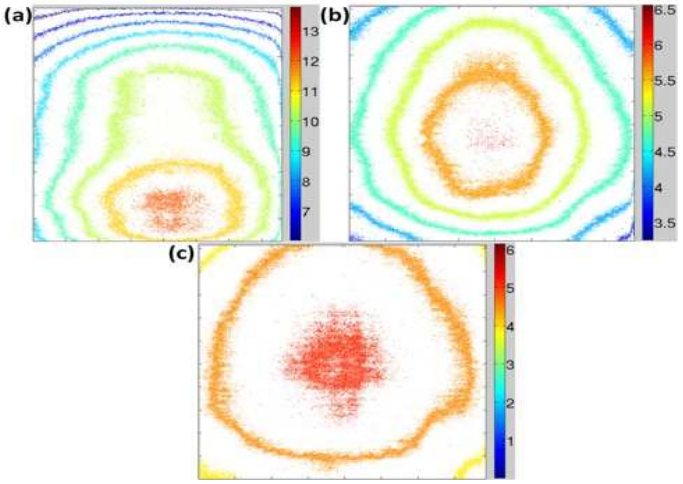

Figure2.5 A

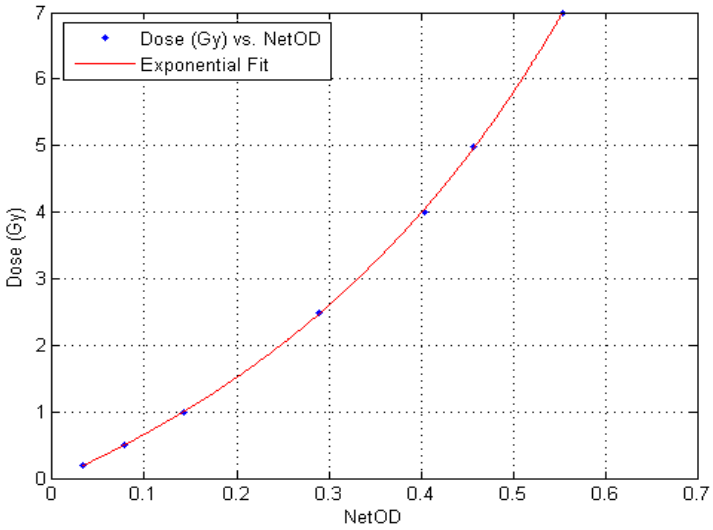

Figure 2.5 B

Figure 2. 5 A. Isodose curves for each irradiator drive shaft position. (a) Position 1, (b) Position 2, and (c) Position 3. The color bars are given in units of Gray units [Gy]. B: Plot of NetOD versus Dose (Gy) at Position 3. A two-term exponential function was fit to the data points.

After the irradiator dose calibration, we can calculate the irradiation dose for each position in the irradiation chamber. For the position 3, the corresponding radiation dose with exposure times of 3, 7, 15, and 30 minutes were calculated to be 5.85, 13.65, 29.25 and 58.5 Gy, respectively, as shown in Table 1.

Table 1. Dose Delivered from Cs-137 exposure.

Exposure Time (mins)	Dose Delivered (Gy)
30	58.5
15	29.25
7	13.65
3	5.85

2.3.2 Cerenkov Radiation Generated from Cs-137 Irradiator

Due to the extremely small number of Cerenkov optical photons, we could not measure the emission spectra with the EMCCD camera. We have observed lots of photons with PMT and oscilloscope. The measured photon pulses are plotted in Fig. 2.6 for the measurement time of 60 seconds. The vertical axis indicates the PMT output voltages, whose values indicate the photon numbers. The horizontal axis indicates the relative measurement time. The rightmost plot with lower output voltages indicates ignorable background photons when the irradiator is off. The voltage jump at time of -25 seconds indicates the power on status.

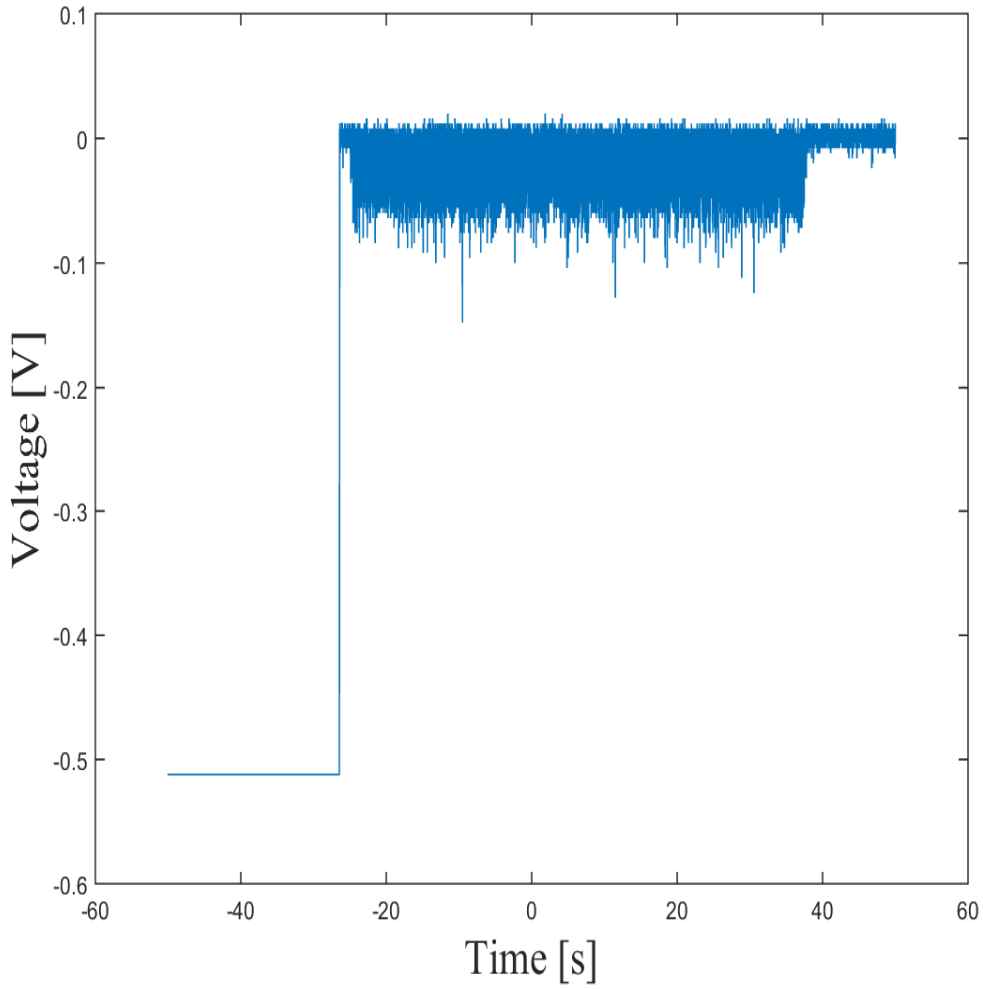

Figure 2. 6 Measuring optical photons from water phantom with Photomultiplier tube (PMT) and oscilloscope.

2.3.3 Cerenkov Radiation Excited PDT *In Vitro*

Figure 2.7 A shows the cell viability in black cell culture plates with irradiation by the Cs-137 irradiator for 30 min and without irradiation. From left to right, each column of the black cell culture plates was treated with different concentrations of the photosensitizer. Compared with the results without irradiation (black triangles), the cell tends to lose its viability with higher MPPa concentration which indicates for Cerenkov radiation induced PDT, the photosensitizer concentration is the main factor. Fig. 2.7 B shows the stained cancer cell organelles. The imaging of the top row represented endoplasmic reticulum (ER) and the bottom row was another subcellular fraction: Mitochondria. Left column in red is

the MPPa image; the middle column in green is the organelle image; the right column is the merged of two images. The cancer cell imaging results of the stained cell organelles, which indicates that MPPa targets both ER and mitochondria as indicated by the color of yellow on the right.

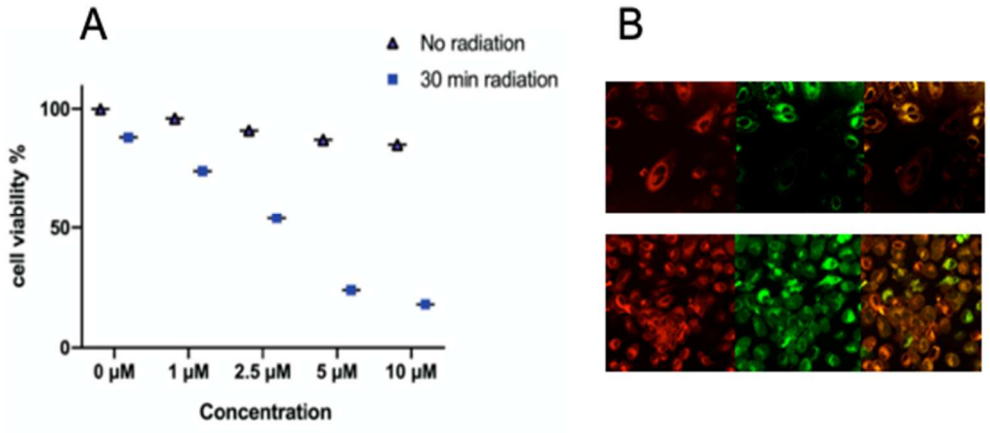

Figure 2. 7 A: The Cs-137 irradiator excited PDT using different concentrations of photosensitizer. B: Stained images showed Organelle staining and imaging for ER (top row) and Mitochondria (bottom row). Left column is MPPa image; middle column is the organelle image; right column is merged.

The cell viability after all plates were irradiated by either the Cs-137 irradiator or laser with different irradiation times using 2.5 μM of MPPa are shown in Fig. 2.8 where the laser treated group was on the left column. We can see that the cell viability is above 85% with the maximum 30 min radiation time. The right column indicates the cell viability when the cells were treated with the high-energy photons. These columns plot the results of Cerenkov radiation excited PDT with different radiation times thus different radiation doses. For the group irradiated for 30 min, we see that the cell viability is 57% as indicated by the rightmost column. The results showed that the efficiency of Cerenkov radiation activated PDT group was higher than optical photon activated PDT group. It confirmed that the Cerenkov radiation induced PDT can achieve excellent therapeutic efficacy.

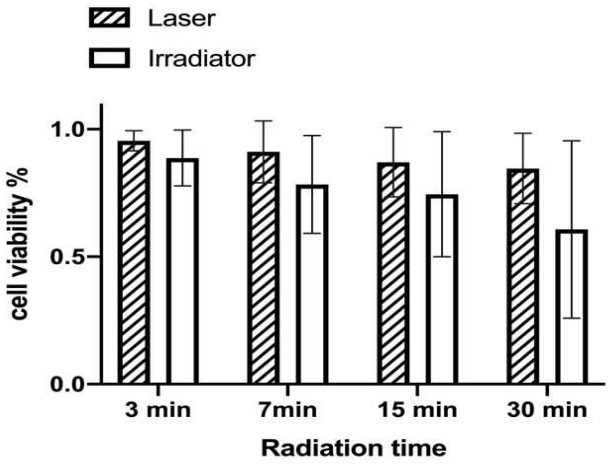

Figure 2. 8 Cell viability (%) of A549 cells after treated by 2.5 μM MPPa photosensitizer and irradiated by the Cs-137 irradiator and laser beam. $p < 0.05$.

2.4 Conclusion

In our studies, we found it was possible that the second-generation photosensitizer, Pyropheophorbide-a methyl ester (MPPa), can be directly excited by high energy γ-rays through Cerenkov radiation without being bundled to any nanoparticles. Our preliminary finding suggests that high energy excited PDT can expand the applications of PDT to the deep tumors inside of the human body due to the greater penetration power of the high-energy photons. No nanoparticles are needed in our approach, which will make the proposed approach more feasible for future clinical applications because there are no nanoparticle toxicity issues. To validate this significant finding, in this work, we used a Cs-137 irradiator as PDT excited light sources to excite MPPa administered to cultured lung cancer cells. Our results have indicated that the high energy excited PDT could treat deep cancer alone or can be used as a complementary treatment option with the radiotherapy, in which the high-energy photons excite the photosensitizer to reduce the radiotherapy time for less side-effects from radiation.

References

[1] Centers for Disease Control and Prevention (CDC) and the National Cancer Institute (NCI) *"United States Cancer Statistics: 1999–2014 Incidence and Mortality Web-based Report,"* <https://nccd.cdc.gov/uscs/> (2014)

[2] The American Cancer Society medical and editorial content team. "Key statistics for Lung Cancer," <https://www.cancer.org/cancer/non-small-cell-lung-cancer/about/key-statistics.html> (2017)

[3] Schouten, L. J., Jager, J. J., van den Brandt, P.A., "Quality of cancer registry data: a comparison of data provided by clinicians with those of registration personnel." Br J Cancer. 68, 974-977 (1993).

[4] Mass, H. A. A. M., Lemmens, V. E. P. P., Nijhuis, P. H. A. *et al*. "Benefits and drawbacks of short-course preoperative radiotherapy in rectal cancer patients aged 75 years and older." EJSO. 39, 1087-1093 (2013).

[5] Lipson, R. L. and Baldes, E. J., "The photodynamic properties of a particular hematoporphyrin derivative." Arch. Dermatol. 82, 508-516 (1960).

[6] Lipson, R. L., Baldes, E. J. and Olsen, A. M., "The use of a derivative of hematoporphyrin in tumor detection." J. Natl cancer Inst. 26, 1-11 (1961).

[7] Foote, C. S., "Mechanism of photosensitized oxidation." Science. 162, 963-970 (1968).

[8] Wilson, B. C. and Patterson, M. S., "The physics, biophysics and technology f photodynamic therapy." Phys. Med. Biol. 53, 61-109 (2008).

[9] Dougherty, T. J., Gomer, C. J., Henderson, B. W., *et al*. "Photodynamic Therapy" J Natl Cancer Inst. 90, 889-905 (1998).

[10] Wan, S., Anderson, R. and Parrish J., "Analytical modeling for the optical properties of the skin with *in vitro* and *in vivo* applications." J Photochem. photobiol. 34, 493-499 (1981).

[11] Wilson, B. C., Patterson, M. and Burns D. M., "Effect of photosensitizer concentration in tissue on the penetration depth of photoactivation light." Laser Med. Sci. 1, 235-243 (1986).

[12] Salgado, D. M. R., Noro-Filho, G. A., Cortes, A. *et al.* "Effect of photodynamic therapy with malachite green on non-surgical periodontal treatment in HIV patients: a piolt spilt-mouth study." Laser Med. Sci. 1,1-5 (2016).

[13] Ferreira, J., Moriyama, L.T., Kurachi C., *et al*. "Experimental determination of threshold dose in photodynamic therapy in normal rat liver." Laser Phys. Lett. 4, 469-475 (2007).

[14] Cherenkov, P. A. "Visible emission of clean liquids by action of γ radiation" Doklady Akademii Nauk SSSR. 2, 451 (1934)

[15] Robertson, R., Germanos, M. S., Li, C., Mitchell G. S., Cherry S. R., Silva, M. D. “Optical imaging of Cerenkov light generation from positron-emitting radiotracers” Phys Med Biol. 54, 355-365 (2009)

[16] Mitchell, G. S., Gill, R. K., Boucher, D. L., Li, C., Cherry, S. R. "In vivo Cerenkov luminescence imaging: A new tool for molecular imaging". Philos. Trans A Math Phys Eng Sci. 369, 4605-4619 (2011)

[17] Jarvis, L. A., Zhang, R., Gladstone, D. J., *et al*. “Cherenkov Video Imaging Allows for the First Visualization of Radiation Therapy in Real Time.” Int J Radiat Oncol Biol Phys. 89, 615–622 (2014)

[18] Kotagiri, N., Sudlow, G. P, Akers, W. J., and Achilefu, S. “Breaking the depth dependency of phototherapy with Cerenkov radiation and low-radiance-responsive nanophotosensitizers.” Nat Nanotechnol. 10, 370-379 (2015)

[19] Tsai, S-M., Bangalore, P., Chen, E.Y., Lu, D., Chiu M-H, Suh A., et al. Graphene-induced apoptosis in lung epithelial cells through EGFR. Journal of Nanoparticles Research. 19, 262 (2017).

[20] Olennick, N. L., Morris, R. L. and Belichenko, I., “The role of apoptosis in response to photodynamic therapy: what, where, why and how.” Photochem. Photobiol. Sci. 1,1-21 (2002).

CHAPTER 3

COMBINATION OF PHARMACEUTICAL AGENTS FOR BETTER TARGETED CANCER THERAPY

3.1 Introduction

Irinotecan, a camptothecin derivative, is approved for treatment of pancreatic and other cancers. This S-phase–specific chemotherapeutic agent inhibits topoisomerase I action by binding to topoisomerase–DNA complexes, preventing DNA relegation, causing DNA-strand breaks, and leading to cell death. Due to the lone pairs, the nitrogen- containing camptothecin derivatives are industrially protonated by forming salts with relevant medicinal acids to further improve their water solubility and minimize the toxicity (Fig. 1b). However, one common problem for all the derivatives of camptothecin is that they undergo pH-dependent lactone hydrolysis to get pharmacologically inactive carboxylate forms which show little topoisomerase inhibitory activity [1,2]. Besides, these camptothecin derivatives also cause many side effects, such as the vascular discomfort due to the low pH value (pH 3.5) of their commercial injections and the severely life-threatening diarrhea [3].

Curcuminoids (Fig. 1c) are linear diarylheptanoids extracted from Curcuma longa. They exhibit many pharmacological effects and have been reported to attenuate cell resistance [4,5], ameliorate gastro- intestinal toxicity [6], protect heart tissue [7] and also possess anti-tumor activities [8,9]. However, the applications of curcuminoids are heavily limited due to their extremely poor water solubility.

So far, no nano formulations based on these two molecular species have been reported. For the first time, we propose a strategy for the construction of easy manufactured drug self-delivery systems based on molecular structures, which can be used for the co-delivery of curcuminoids and all the nitrogen-containing derivatives of camptothecin for better targeted cancer therapy via charge conversion. The formation mechanism investigation demonstrates that the two molecular species can self-assemble into complex ion pairs in polar organic solvents through intermolecular non-covalent interactions, resulting in a uniform distribution with certain molar ratios before being penetrated into anti-solvents to form nanoparticles. As shown in Scheme 1, these nanoparticles show stabilized particle sizes (100 nm) under various conditions and tunable surface charges which increase from around −10mV in a normal physiological condition (pH 7.4) to +40 mV under acidic tumor environments. The water solubility of curcuminoids is dramatically improved and the lactone hydrolysis of camptothecin derivatives is also restricted to keep their

pharmacologically active forms. Besides, the formulation with a pH value close to that of normal blood would reduce the side effects caused to blood vessels and improve the patient compliance compared to commercial injections of camptothecin derivatives (pH 3.5). More importantly, in vivo mice experiments have confirmed that, compared to irinotecan itself, the co-delivered irinotecan curcumin nanoparticles exhibited dramatically enhanced lung and gallbladder targeting, improved macrophage-clearance escape and better colorectal cancer treatment with an eradication of life-threatening diarrhea, which brings great hope for better targeted chemotherapy and clinical translation. The strategy of construction of drug self-delivery systems based on molecular structures may inspire more discoveries of similar formulations for wider pharmaceutical applications.

3.2 Methods and Materials

3.2.1 Chemical Reagents

Irinotecan hydrochloride, topotecan hydrochloride, curcumin, poloxamer 105, mannitol, glucose, paraformaldehyde and dimethyl sulfoxide (DMSO) were purchased from Sigma-Aldrich and used as received. Wortmannin, cytochalasin D, genistein and methyl-β-cyclodextrin were purchased from Meilun Biotechnology Co. Ltd (Dalian, China). Chlorpromazine was obtained from Selleck Chemicals (China). Phosphate buffered saline (PBS, pH = 7.4) was prepared in the lab and ultrapure water was produced using a Milli-Q integral water purification system.

3.2.2 Cells and Animal Models

HT-29 colorectal adenocarcinoma cells were obtained from Boster Biological Technology Co. Ltd (Hubei, China). Male BALB/c nude mice, aged 5 weeks (18–22 g, SPF grade), were purchased from Dashuo experimental animals Co., Ltd. (Chengdu, China). All animal experiments were conducted under the guidelines approved by the Institutional Animal Care and Use Committee (IACUC) of Chengdu University of Traditional Chinese Medicine.

3.3.3 *In Vivo* Therapeutic Efficacy

HT-29 cell suspension (2×10^6 cells per 200 μL) were subcutaneously injected into the flank of male BALB/c mice. When tumor volume reached around 100 mm3, the HT-29 tumor bearing nude mice were randomly divided into three groups (four or five mice for each group) and were intravenously injected with PBS, irinotecan hydro- chloride (27.5 mg/kg/mouse) or SICN (equivalent irinotecan 27.5 mg/ kg/mouse) every other day for consecutive 20 days. Tumor volume was measured every third day and calculated according to the formula: Tumor volume = length x width^2/2. Mice were weighted every three days and the severity of diarrhea was scored according to the following standards [10]: 0 (normal, normal stool or absent); 1 (slightly wet and soft stool); 2 (moderate, wet and unformed stool with moderate peri- anal staining of the coat); and 3 (severe, watery

stool with severe perianal staining of the coat). Mice were sacrificed after 5 days of medication discontinuation. Tumors were excised, weighted and photographed. The excised tissues (heart, liver, spleen, lung, kidney, brain and tumor) were fixed in 4% paraformaldehyde to prepare paraffin sections. Hematoxylin/eosin (H&E) staining was used for histological analysis.

3.3.4 *Ex Vivo* biodistribution

Mice with subcutaneous tumors of around 100 mm^3 were intravenously injected with irinotecan hydrochloride or SICN (equivalent irinotecan 27.5 mg/kg/mouse). Fluorescence based visual distribution of drugs and their average signal on excised tissues were obtained on a FUSION FX7 live animal imaging system.

3.4 Results

3.4.1 Nanoparticle Morphology

The morphologies of evaporated SICN nanoparticles and their lyophilized powder with mannitol were characterized by SEM. For the evaporated SICN, spherical particles with smooth surfaces are displayed in Fig. 3.1 A and their sizes are similar to those in suspension (around 100 nm). he apparent appearance of SICN and curcumin in water is shown in Fig. 3.1B Compared to pure curcumin in water, the water solubility of curcumin is markedly improved by forming nanoparticles with irinotecan hydrochloride.

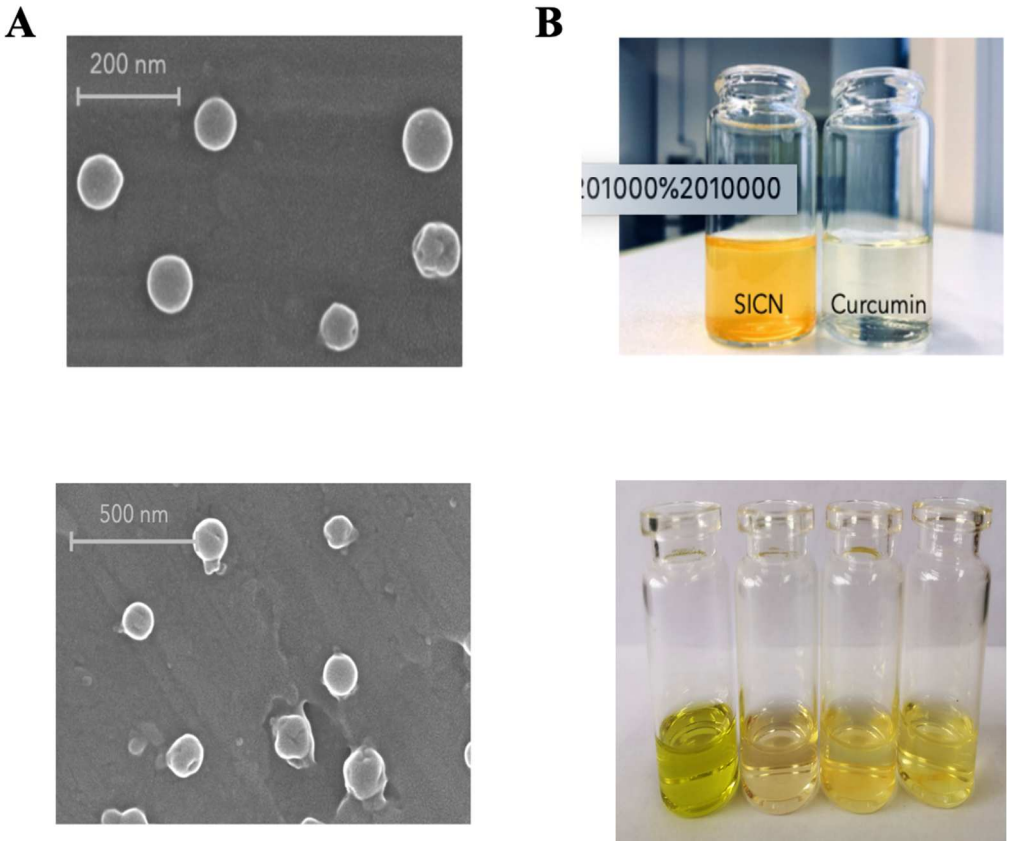

Figure 3.1 Morphologies of nanoparticles. (a) Particle sizes of ICN increase from about 70 nm to 100 nm in PBS (b) Apparent appearance of SICN and curcumin in water exhibits the dramatically improved water solubility of curcumin by forming nanoparticles with irinotecan hydrochloride

3.4.2 Nanoparticle Formation Mechanism

Camptothecin is a natural hydrophobic alkaloid with multiple conjugated aromatic rings and rigid planar structure (Fig. 3.2), allowing it to sustain the DNA/topoisomerase complex and to subsequently result in cell death. Due to the lone pairs, the nitrogen- containing camptothecin derivatives are industrially protonated by forming salts with relevant medicinal acids to further improve their water solubility and to minimize the toxicity. The extremely poor water-solubility of curcumin and camptothecin (the parent compound of irinotecan), the relatively exposed hydrogen atoms and the rigid planar structures (Fig. 3.1) of both molecules with multiple conjugated aromatic rings provide the possibility of hydrophobic inter- actions, hydrogen bonding and π-π stacking between these two molecules, respectively.

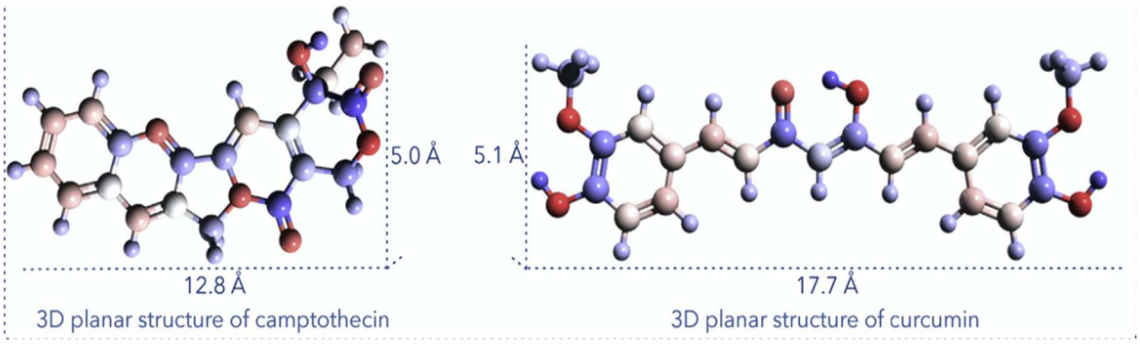

Figure 3. 2 Three-dimensional grid planar structures and sizes of camptothecin and curcumin

3.4.3 *In Vitro* Cytotoxicity and Cellular Uptake

The in vitro cytotoxicity and fluorescence-based cellular uptake efficiency of SICN nanoparticles under various environmental pH values were explored on HT-29 cells. As shown in Fig. 3.3, the half maximal inhibitory concentration (IC50) of irinotecan hydrochloride on cells under normal environment (pH 7.4) is 15.25 μM. The IC50 of SICN nanoparticles on cells with environmental pH of 7.8, 7.4 and 6.5 are 0.278 mg/mL, 0.112 mg/mL and 0.019 mg/Ml, equaling to 7.720 μM, 3.112 μM and 0.537 μM of irinotecan hydrochloride, respectively. Significant difference between groups at every dosage level is obtained ($p < 0.001$). Compared to the free irinotecan hydrochloride, the in vitro cytotoxicity of SICN is significantly improved by forming nanoparticles. Besides, the acidic environments could result in greater in vitro cytotoxicity of SICN on HT- 29 cells than the alkaline condition because of the conversional positive surface charges of nanoparticles under tumor environments and the negative surface charges under normal physiological conditions.

The fluorescence-based cellular uptake of SICN nanoparticles under different environmental pH values are shown in Fig. 3.4. The blank group, namely cells under normal conditions without SICN nanoparticles, shows no fluorescence. For SICN groups, cells under acidic environments exhibit significantly stronger fluorescence than those in alkaline conditions ($p < 0.001$), demonstrating the higher uptake efficiency of SICN under tumor environments.

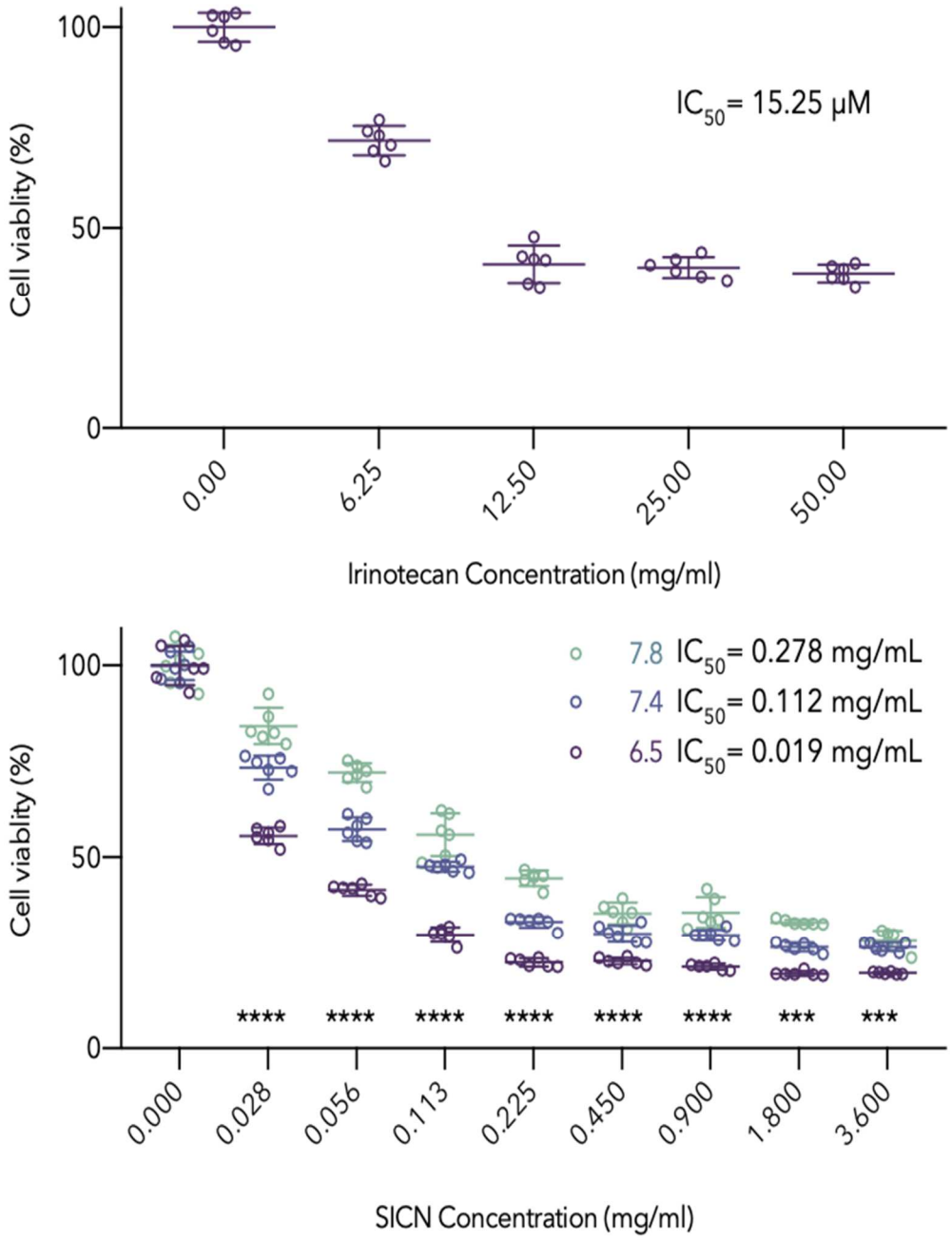

Figure 3. 3 MTT assay of irinotecan hydrochloride and SICN nanoparticles by changing environmental pH values on HT-29 cell line IC50: Half maximal inhibitory concentration; SICN: surfactant stabilized irinotecan hydrochloride curcumin nanoparticles; ***, $p < 0.001$; ****, $p < 0.0001$.)

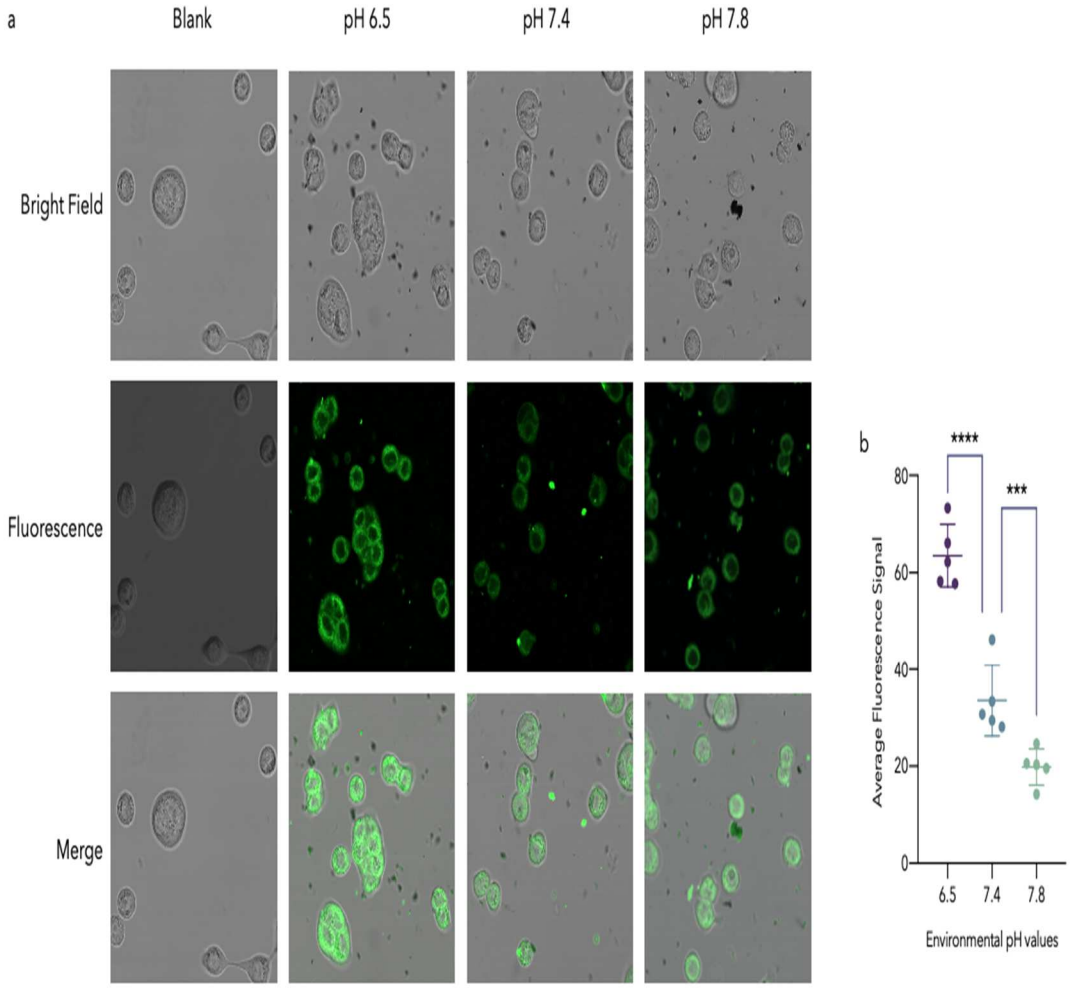

Figure 3. 4 Fluorescence based distribution and uptake of SICN nanoparticles under different environmental pHs. (a) Blank group, namely cells under normal condition without adding SICN nanoparticles, shows no fluorescence. For groups adding SICN nanoparticles, cells under acidic environment (pH 6.5) shows stronger fluorescence than those under alkaline environments (pH 7.4 and pH 7.8), demonstrating the higher uptake of SICN under acidic environments; (b) The significant difference between groups with different environmental pH values. Data represent the mean ± SD. (*, $p < 0.001$; ****, $p < 0.0001$)**

3.4.4 Plasma Concentration

The plasma concentration-time profiles of free irinotecan hydrochloride and SICN nanoparticles are shown in Fig. 3.5. The plasma concentration for irinotecan hydrochloride

group decreases by around 80% after 2 h while the concentration for SICN group still keeps at about 50% in plasma. Mice receiving a single injection of SICN nanoparticles achieve an obvious improvement in plasma concentration and exposure compared to free irinotecan.

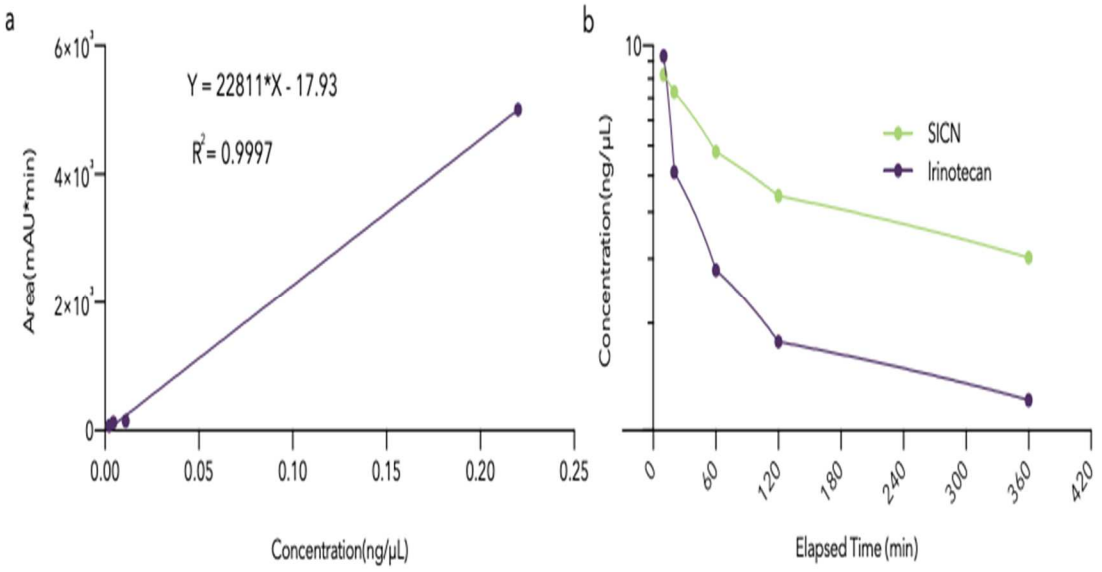

Figure 3. 5 Calibration curves with a regression equation for quantification of irinotecan (a) and plasma concentration-time profile of SICN nanoparticles after a single i.v. administration in nude mice compared to irinotecan hydrochloride.

3.4.5 *In vivo* Therapeutic efficacy

The anti-tumor effect of SICN nanoparticles was invested on HT-29 subcutaneous xenograft nude mice. The experimental strategy is illustrated in Fig. 3.6 a. Compared to the PBS group, the average tumor volumes of mice in medication groups are effectively controlled and significant difference occurs on day 9 (around a week post first administration, Fig. 3.6 b). The regression of tumor volume in the medication groups occurs on day 15 (around two weeks post first administration). The medication groups also show significant differences in tumor weight (Fig. 3.6 d) and the photography of excised tumors is shown in Fig. 3.6 e. No statistical difference between the two medication groups occurs during the whole experiment. These results confirm that the SICN nanoparticles are as equally effective in colorectal cancer treatment as free irinotecan hydrochloride and the tumor regression effect of SICN is caused by irinotecan instead of curcumin. This should be attributed to the significant difference in half maximal inhibitory concentration of the two molecules. Curcumin can be generally regarded as a biosafe molecule at the dose level.

No significant loss of body weight was observed in all the mice during the whole experiment, indicating the negligible side effects of the SICN nanoparticles for tumor

therapy at the employed dose (Fig.3.6 f). Besides, the H&E staining images of tumors and major organs (heart, liver, spleen, lung, kidney and brain) from HT-29 tumor-bearing mice treated with PBS, free irinotecan or SICN are shown in Fig. 3.6 g. Except for the glandular cavities, the H&E staining of colon cancer sections from the PBS group shows intact tumor cell structure. Cells exhibit distinct nuclei with a nearly spherical thin cytoplasmic region. H&E-stained sections of colon cancer from medication groups have distinct damage of tumor cell nuclei and distorted membranes sur- rounding necrotic tissues. However, compared to the PBS treated group, neither noticeable organ damage nor inflammation lesion can be observed in the medication groups, indicating the negligible organ dysfunction after being treated with SICN nanoparticles or irinotecan. All these results demonstrate that the SICN nanoparticles exhibit high biosafety for cancer treatment presenting no significant side effects to the treated mice.

As shown in Fig. 3.6 h, significant delayed diarrhea in the mice treated with free irinotecan occurs on day 10 (10 days post first administration, $p < 0.01$) while no obvious diarrhea is observed in PBS or SICN treated group during the whole experiment, demonstrating the presence of curcumin in the nano formulation could protect the intestine and ameliorate the gut toxicity by alleviating diarrhea in mice. This can be due to whether the protective effects of curcumin molecule [11] or the formulation changes of irinotecan with the help of curcumin.

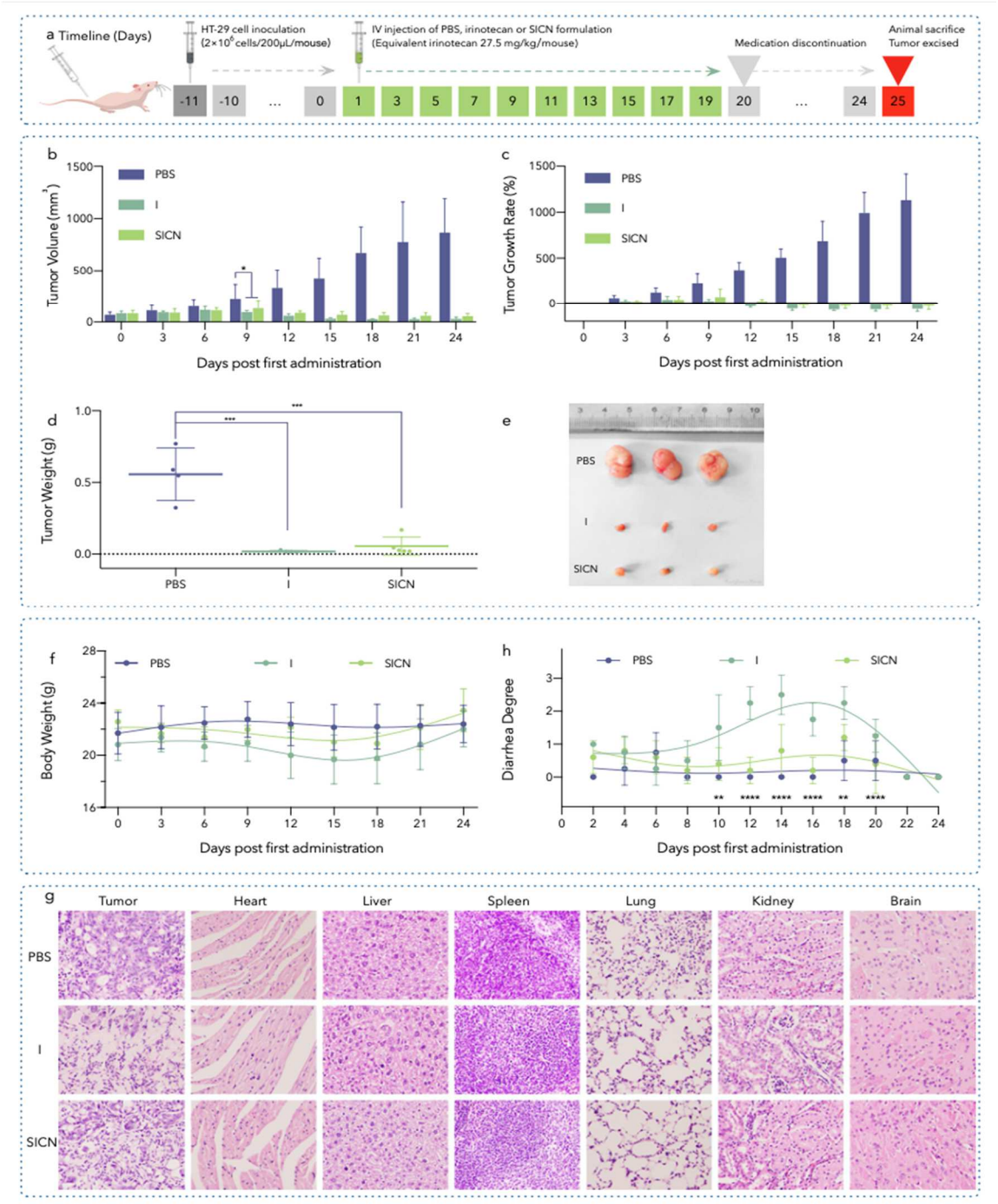

Figure 3. 6 Anticancer efficacies of SICN on HT-29 subcutaneous xenograft nude mice. (a) A schematic diagram of the experimental design of anticancer efficacy; (b) Tumor volume (b), tumor growth rate (c), tumor weight (d) and tumor images (e) from mice treated with PBS, I or SICN; (f) Negligible changes of Body weight; (g) H&E staining images of excised tumors and major organs (magnification of 400x). (h) Delayed diarrhea degree of mice (significant difference between SICN and I treated groups, no statistical difference between SICN and PBS treated groups) Surfactant stabilized Irinotecan hydrochloride and Curcumin Nanoparticles. Significance of differences between groups are analyzed using 2way ANOVA. * p < 0.05, ** P < 0.01, *** P < 0.001, **** P < 0.0001.

3.4.6 *Ex Vivo* Biodistribution

The ex vivo biodistribution investigation was carried out according to Fig. 3.7 a. The normalized fluorescence spectra of irinotecan hydro- chloride in water containing 50% of DMSO (Fig. 3.7 b) and SICN in PBS (Fig. 3.7 c) show that irinotecan in both forms display similar fluorescence behavior with an excitation maximum at around 370 nm and an emission maximum at about 430 nm. The fluorescence based biodistribution of irinotecan hydrochloride and SICN on excised tissues are shown in Fig. 3.7 d and e, respectively. Except for the high accumulation of irinotecan hydrochloride in tumors (Fig. 3.7 d), a relatively higher biodistribution in the liver can also be observed. Their relatively average signals are 27% and 37%, respectively (Fig. 3.7 f. Compared to irinotecan hydrochloride, a visually higher accumulation of SICN in tumor is observed and its relatively average signal figures prominently (36% in Fig. 3.7g, around 33% larger than that of free irinotecan, 27% in Fig. 3.7 f), showing an improved tumor targeting of SICN. Besides, the relative accumulation of SICN in the liver is lower (18% in Fig. 3.7 g) than that of free irinotecan (37% in Fig. 3.7 f), which might also be one of the reasons that relieve the side effects. Clinically, the severe diarrhea caused by irinotecan hydrochloride is due to the biliary elimination and the subsequent microbiome reactivation in intestines [12,13]. Therefore, except for the protective effect of curcumin on intestines [11], the diarrhea alleviation effect of SICN could also be attributable to the improved tumor targeting, which relatively reduces their quick accumulation in liver and lessens the chances of being rapidly metabolized and excreted into intestines.

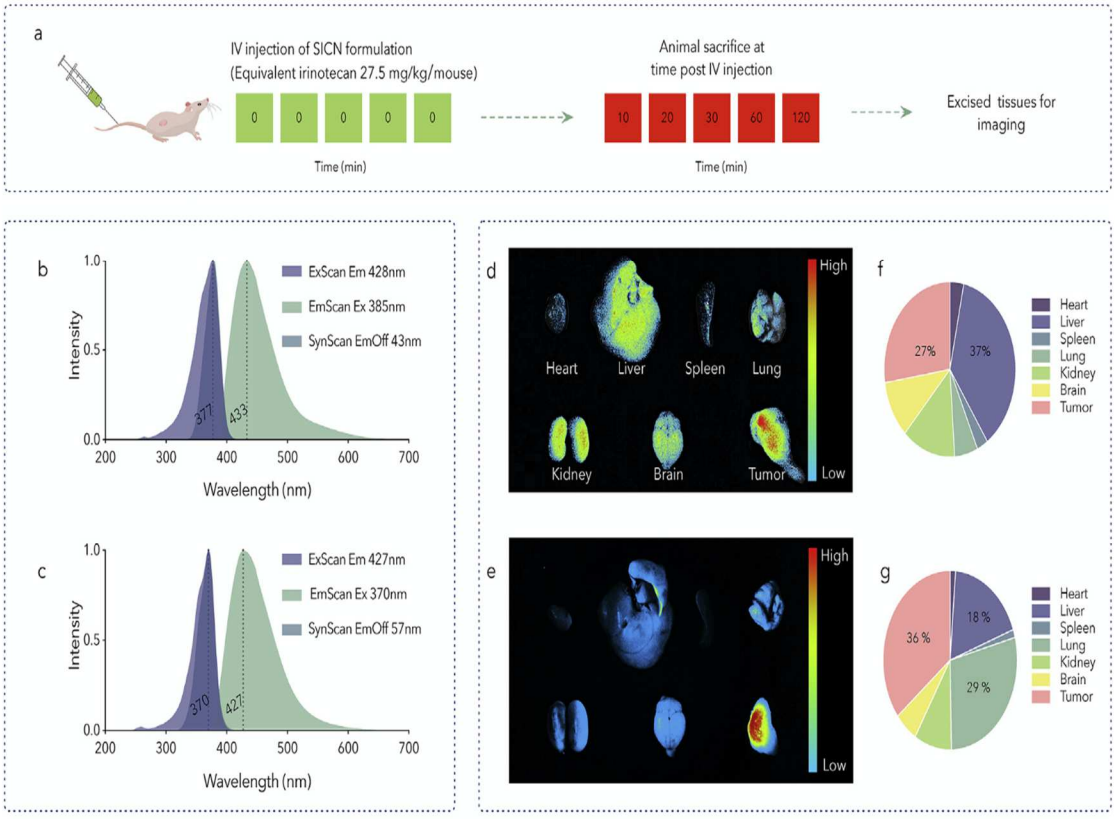

Figure 3. 7 Distribution of SICN nanoparticles on HT-29 subcutaneous xenograft nude mice. (a) A schematic diagram of the experimental design of ex vivo biodistribution by using HT-29 tumor-bearing nude mice; Irinotecan hydro- chloride in water containing 50% of DMSO (b) and SICN in PBS (c) exhibit similar behavior in their normalized fluorescence spectra; Fluorescence based relative biodistribution of irinotecan hydrochloride (d) and SICN nanoparticles (e) on tissues from mice sacrificed at 10 min post intravenous injection; The relatively average signal of irinotecan hydrochloride (f) and SICN nanoparticles (g) on excised tissues.

3.5 Conclusion

two molecular species can self-assemble into complex ion pairs in polar organic solvents through intermolecular non-covalent interactions, resulting in a uniform distribution of them before being penetrated into anti-solvents to form nanoparticles. These nanoparticles show stabilized particle sizes (100 nm) with mono distribution. The water solubility of curcuminoids is dramatically improved and the lactone hydrolysis of camptothecin derivatives is also restricted to keep their pharmacologically active forms. Besides, the formulation with a pH value close to that of normal blood would reduce the side effects caused to blood vessels and improve the patient compliance compared to commercial injections of camptothecin derivatives (pH 3.5). More importantly, *in vivo* mice

experiments have demonstrated that, compared to irinotecan itself, the co-delivered irinotecan curcumin nanoparticles exhibited dramatically enhanced lung and gallbladder targeting, improved macrophage-clearance escape and ameliorated colorectal cancer treatment with an eradication of life-threatening diarrhea, exhibiting great promise for better targeted chemotherapy and clinical translation.

References

[1] S. Palakurthi, Challenges in SN38 drug delivery: current success and future directions, Expert Opin. Drug Deliv. 12 (12) (2015) 1911–1921.

[2] T. Y. Ci, T. Li, G.T. Chang, L. Yu, J.D. Ding, Simply mixing with poly(ethyleneglycol) enhances the fraction of the active chemical form of antitumor drugs of camptothecin family, J. Control. Release 169 (3) (2013) 329–335.

[3] F. N. U. A.U. Rahman, S. Ali, M.W. Saif, Update on the role of nanoliposomal irinotecan in the treatment of metastatic pancreatic cancer, Therap. Adv. Gastroenterol. 10 (7) (2017) 563–572.

[4] P. Su, Y. Yang, G. Wang, X. Chen, Y. Ju, Curcumin attenuates resistance to irinotecan via induction of apoptosis of cancer stem cells in chemoresistant colon cancer cells, Int. J. Oncol. 53 (3) (2018) 1343–1353.

[5] M. Murakami, S. Ohnuma, M. Fukuda, E.E. Chufan, K. Kudoh, K. Kanehara, N. Sugisawa, M. Ishida, T. Naitoh, H. Shibata, Y. Iwabuchi, S.V. Ambudkar, M. Unno, Synthetic analogs of curcumin modulate the function of multidrug re- sistance–linked ATP-binding cassette transporter ABCG2, Drug Metab. Dispos. 45 (11) (2017) 1166–1177.

[6] J. J. Johnson, H. Mukhtar, Curcumin for chemoprevention of colon cancer, Cancer Lett. 255 (2) (2007) 170–181.

[7] O. Ciftci, N.B. Turkmen, A. Taslıdere, Curcumin protects heart tissue against ir- inotecan-induced damage in terms of cytokine level alterations, oxidative stress, and histological damage in rats, Naunyn Schmiedeberg's Arch. Pharmacol. 391 (8) (2018) 783–791.

[8] M. C. Bonferoni, S. Rossi, G. Sandri, F. Ferrari, Nanoparticle formulations to enhance tumor targeting of poorly soluble polyphenols with potential anticancer properties, Semin. Cancer Biol. 46 (2017) 205–214.

[9] J. Adiwidjaja, A.J. McLachlan, A.V. Boddy, Curcumin as a clinically promising anti- cancer agent: pharmacokinetics and drug interactions, Expert Opin. Drug Metabol. Toxicol. 13 (9) (2017) 953–972.

[10] A. Kurita, S. Kado, N. Kaneda, M. Onoue, S. Hashimoto, T. Yokokura, Modified irinotecan hydrochloride (CPT-11) administration schedule improves induction of delayed-onset diarrhea in rats, Cancer Chemother. Pharmacol. 46 (3) (2000) 211–220.
[11] J. J. Johnson, H. Mukhtar, Curcumin for chemoprevention of colon cancer, Cancer Lett. 255 (2) (2007) 170–181.
[12] Y. Pommier, M. Cushman, J.H. Doroshow, Novel clinical indenoisoquinoline to poisomerase I inhibitors: a twist around the camptothecins, Oncotarget 9 (99)
(2018) 37286–37288.
[13] L. Guthrie, S. Gupta, J. Daily, L. Kelly, Human microbiome signatures of differential colorectal cancer drug metabolism, Npj Biofilm. Microbiol. 3 (2017).

CHAPTER 4

PHOTODYNAMIC THERAPY SYNERGIZED WITH CHEMOTHERAPY TO ENHANCE ANTI-TUMOR EFFICACY

4.1 Introduction

The ability of tumor cells to adapt to therapeutic regimens by activating alternative survival and growth pathways remains a major challenge in cancer therapy. Therefore, the most effective treatments will involve interactive strategies that target multiple nonoverlapping pathways while eliciting synergistic outcomes and minimizing systemic toxicities. The combination therapy strategy has already been utilized in the clinic, known as drug cocktail therapy. Studies have found that multi-pronged assault to tumors through administering a cocktail of different anti-cancer agents could achieve synergistic anti-tumor efficacy and minimize the severe side effects compared to the respective mono-therapeutic [1].

Recently, photodynamic therapy (PDT) is widely recognized as a promising alternative cancer treatment modality due to its painless and noninvasive administration process [2]. During the treatment, a photosensitizer is administered to patients and followed by the illumination with a light source at the tumor site. The light can activate the photosensitizer localized in the tumor site and then react with intracellular oxygen to form cytotoxic reactive oxygen species (ROS) [3]. Based on the PDT process, it can eradicate tumor tissue at low risk and in a controlled manner. The side effect of PDT is relatively low because it is believed that the photosensitizer is not toxic until excited by the light. The major limitation is the challenges in delivering the light into deep tumors due to strong optical scattering and absorption. One strategy to overcome this limitation is to use high energy photons like x-rays to excite the photosensitizers [4]. Another approach is to use a light guidance or catheter to deliver light into deep tissues directly [5].

Curcuminoids are bioactive compounds obtained from the plant Curcuma longa. One of its bioactive ingredient curcumin has been used as the photosensitizer of PDT [6,7]. Curcuminoids have many features, such as the blue region absorption, the long-wavelength cation photo-polymerization, and minimal cell cytotoxicity to normal cells, which make curcumin an ideal candidate as photosensitizers in PDT. Although curcumin has the potential to be a good photosensitizer candidate for efficient PDT, some limitations are preventing it from being widely utilized in the clinic. One drawback is its poor water solubility [8]. Another drawback is its instability under physiological conditions. In our previous study [9], we have reported a straightforward strategy to construct an easy manufactured drug self-delivery system in which two-molecular species Irinotecan and

Curcumin can self-assemble into a complex of ion pairs, through intermolecular non-covalent interactions. The nano-self-assembly has been proven to be effective in delivering aqueous insoluble small molecules so that the water solubility of curcuminoids is improved substantially and the lactone hydrolysis of camptothecin derivatives remain activated in pharmacologically active forms [10].
Our previous work has proved that the nano-self-assembly has better chemotherapy efficacy with much fewer side effects compared with the individual components. However, its efficacy as a PDT photosensitizer has not been explored. And the combination of chemotherapy and PDT using the same nano-self-assembly has not been studied. In this paper, we report our studies on these two studies. Briefly, we would like to introduce ICN as a potent anti-tumor agent. The formulation of ICN is composed of a chemotherapy drug irinotecan and photosensitizer curcumin for combinatorial chemo-photodynamic therapy.

4.2 Methods and Materials

4.2.1 Materials

Irinotecan hydrochloride, curcumin, poloxamer 105, mannitol, dimethyl sulfoxide (DMSO), and DMEM Mixture F-12 Ham (DMEM/F12) were purchased from Sigma-Aldrich (St Louis, MO, USA) and used as received. Phosphate Buffered Saline (PBS, pH = 7.4) was prepared in the lab and ultrapure water was produced using a Milli-Q integral water system (Millipore, MA, USA). MitoTracker Red CMXRos was purchased from Beyotime Biotechnology Inc (P.R. China). Annexin V apoptosis detection kit FITC and ROS detection kit were purchased from KeyGEN Biotech (Nanjing, P.R. China). Penicillin–streptomycin, fetal bovine serum, and trypsin were purchased from Gibco (Grand Island, NY, USA)

4.2.2 Preparation of ICN

ICN was synthesized and purified as described in our paper [11]. Briefly, irinotecan hydrochloride and curcumin nano-cocrystals (ICN) were prepared based on an anti-solvent precipitation method. Typically, irinotecan hydrochloride (6.2 mg) and curcumin (3.7 mg) (Molar ratio I:C is about 1:1) were dissolved DMSO (300 μL) at room temperature, in which 1.5 mg of injectable non-ionic surfactant poloxamer 105 was added. The obtained organic solution was added into ultrapure water (30 mL) with magnetic stirring (500 RPM for 5 min) at room temperature.

4.2.3 Cytotoxicity Assay

HT-29 cells were incubated in DMEM/F12 medium, where 10% FBS and 100 U (per mL) penicillin-S. were added. The cells were then seeded on 96-well plates with a density of 1×104 per well with DMEM/F12 medium and incubated in a humidified incubator containing 5% CO2 at 37 °C for 24 h. After removal of the original medium, the cells were

treated with various concentrations of Curcumin, Irinotecan hydrochloride, and ICNs for 4 h incubation. Then, the cells were washed with PBS and fresh medium twice and then exposed to 480 nm pigtailed laser diodes (80 mW/ cm^2, 5 min). After incubation for 12 h, the cells were incubated with 20 μL MTT (5 mg/mL) for 4 h. Solutions were removed and followed by treatment with 150 μL DMSO to dissolve the formazan crystals. The absorbance was set at 490 nm using Elx800 Universal Microplate Reader (BioTek Instruments Inc., Winooski, VT, USA). The errors were calculated from two independent sets of experiments, in each of which six replicate wells were run for each concentration.

4.2.4 Detection of Intracellular ROS

HT-29 cells were plated in 12-well plates at the density of 1×105 cells per well for 24h at 37°C. After incubation with Curcumin and ICNs (5 μM of free Cur equivalent) for 4 h, the cells were washed twice with PBS buffer to remove excess. Each well was exposed to a 480-nm laser diode (power density 80 mW/cm^2) for 5 min at the same distance to deliver the same power. After incubation for 12 h, the cells were washed. Then 700 μL of 10 μM DCFH-DA was added to the cell suspension and incubated for 20 min at room temperature. The fluorescence signals were measured by flow cytometry and analyzed by Cell Quest software (Becton Dickinson FACSVerse).

4.2.5 Cellular Localization of Drugs

HT-29 cells were seeded on a glass-bottom petri dish at a concentration of 5×10^3 cells (per mL) for 12 h. After that, the cells were incubated with curcumin of 5 μM and ICN (equaling to Cur.) suspension for 4 h. After being washed two times with PBS, the cells were stained with Mito-Tracker Red (0.2 μM) reagent in live-cell imaging solution at room temperature for 30 min. The cells were then washed twice with PBS and placed under Leica SP8 X confocal microscope for imaging. Laser sources at 488 nm and 552 nm were used for the capture of curcumin, ICN, and Mito-Tracker, respectively.

To better identify the visualize the fluorescent confocal microscopy, EBImage toolbox was introduced in this study. EBImage is a very useful tool for analyzing and processing images. This software can be downloaded through the website of bioconductor.org. EBImage package can be installed into R (version 4.0 or higher) to visualize images. This package was firstly introduced by Gregoire Pau and his team form U.K. and German Cancer Research Center, university of Heidelberg, Germany in the year of 2010. And this study was summarized and published in the journal bioinformatics. [12]

4.2.6 Fluorescence-based Distribution and Uptake

HT-29 cells were seeded in confocal dishes and cultured in DMEM/F12 medium for 12 h. ICN suspension (equaling to 50 μM of Irinotecan hydrochloride) was then added into each

dish and incubated in media with pH of 6.7 and 7.5 for 3 h before being measured by a Leica SP8 X confocal laser scanning microscope (excitation wavelength of 488 nm; Emission wavelength of 490- 552 nm)

4.2.7 Apoptosis Analysis

Cell apoptosis was measured using Annexin V–FITC (fluorescein isothiocyanate)/PI (propidium iodide) Apoptosis Assay Kit. HT-29 cells were seeded in 12-well plates for 24 h at the density of 1×105 per well and incubated with 5 μM free Curcumin and ICN for 4 h. Then, each well was washed with PBS buffer twice and exposed to 480 nm laser diode for 5 min (power density 80 mW/cm^2). After incubation for 12 h, the cells were washed and fixed in 500 μL of Annexin V binding buffer containing 5 μL Annexin V-APC and 5 μL PI. After incubated at room temperature for 15 min in the dark, the cells were assessed for the status of apoptosis with FACS Calibur flow cytometer (Becton Dickinson, USA).

4.2.8 In vivo Therapeutic Efficacy

Male BALB/c nude mice, aged 5 weeks (20–24 g), were purchased from Dashuo experimental animals Co., Ltd. (Chengdu, China). All animal experiments were conducted under the guidelines approved by the Institutional Animal Care and Use Committee (IACUC) of Chengdu University of Traditional Chinese Medicine. The HT-29 tumor-bearing mice were randomly divided into three groups (Saline solution, Curcumin, and ICN) with equivalent tumor volume (around 100 mm3), and were injected intravenously irinotecan hydrochloride (0.2μM kg per mouse) or ICN (equivalent irinotecan 0.2μM/kg per mouse) every three days for consecutive 15 days. All mice were fed in a dark room. For PDT experiments, the tumor site was illuminated by a 480-nm light source for 20 mins with a power density of 80 mW/cm2. The PDT was implemented every three days and lasted for 21 days. Tumor volume was measured every third day and calculated as follows: Tumor volume = length × width^2/2. Mice were sacrificed after 7 days of medication discontinuation. Tumors were excised, weighed and photographed.

4.2.9 Statistical Analysis

All quantitative data are shown as mean±SD, n≥3. Statistical analysis was conducted using GraphPad Prism (Version 8.4.0) t-test calculator and *p<0.05, **p<0.01, ***p<0.001. R studio desktop was updated to version 1.3 for macOS. EBImage package (Version 4.32.0) was installed from bioconductor.org.

4.3. Results

4.3.1 In Vitro Cytotoxicity

We first assessed the cytotoxicity of the Irinotecan and ICN induced anti-tumor efficacy in HT-29 cells (Fig. 4.1A). Cell viability studies under two different cancer treatments were performed to estimate cytotoxicity and anti-cancer efficacy on HT-29 cells. A significant

decrease in HT-29 cell survival was observed at low concentrations (< 6.25 μM). However, the cytotoxicity can hit the therapeutic 'plateaus' while doubling the dosage of chemotherapy agents. The ICN group stalled out to 30% of cell viability even when the concentration of ICN increased to 8 times higher (50 μM). To overcome the anti-cancer drug resistance, we investigated the anti-cancer efficacy of Irinotecan and ICN in combination with photodynamic therapy. As shown in Figs. 4.1 B and 4.1 C, with or without laser irradiation, the curcumin group and Irinotecan group exhibited negligible differences in cell cytotoxicity to HT-29 cells in all concentrations. However, after having been exposed to laser, for the treatments with 2.5 μM and 5 μM of ICN, the viabilities of HT-29 cells were 57% and 21%, respectively. When HT-29 cells were treated with 10 μM ICN in the combination of laser-induced PDT, the therapeutic 'plateau' was significantly brought down to 9%. ICN showed great cytotoxicity to HT-29 at low concentration but remained on 'the plateaus' of anti-cancer efficacy of around 33% at high concentration. With the combination of two treatments (ICN+PDT), a huge decrease of HT-29 cell viability was observed in Fig. 4.1 C. This result verified that the combination treatments can achieve better anti-tumor efficacy than an individual treatment alone.

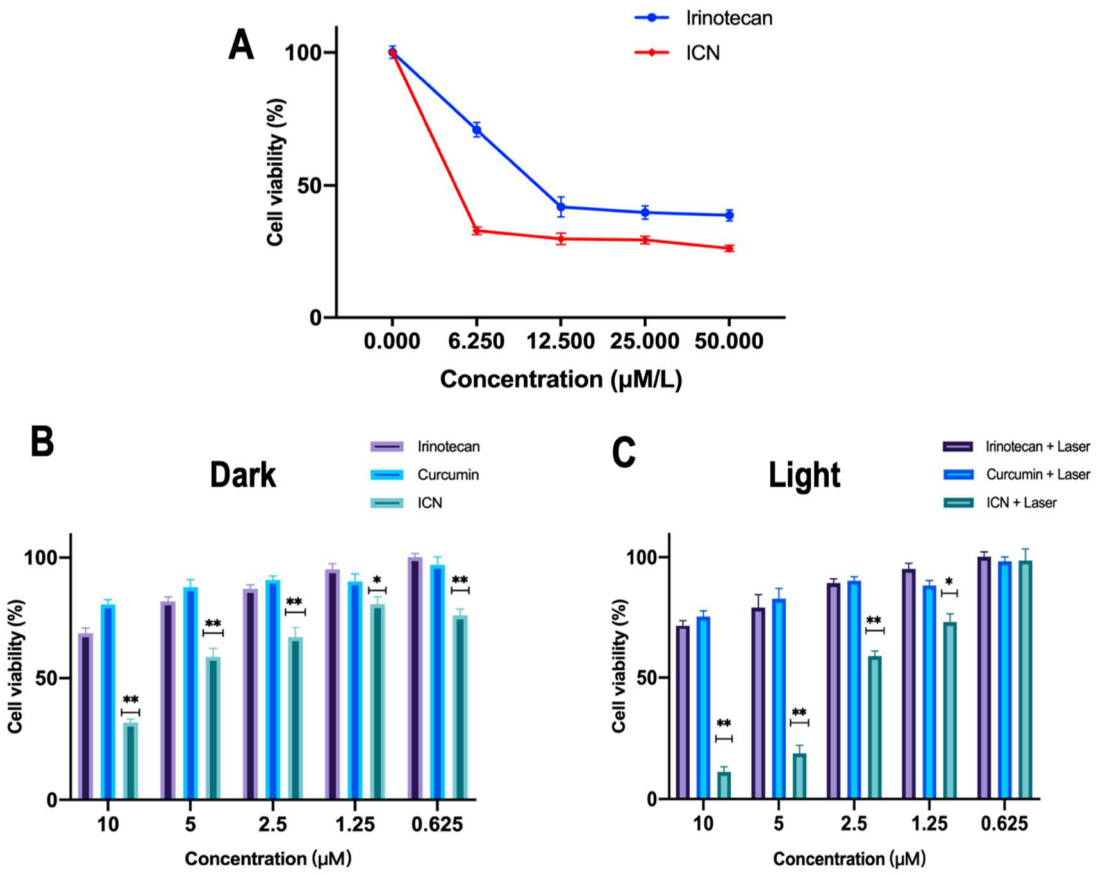

Figure 4. 1 (A) In vitro cytotoxicity of Irinotecan and ICN in HT-29 cells. Cell viabilities of the HT-29 cells treated with Irinotecan, Curcumin, and ICN in the dark (B), and with laser exposure (C).

4.3.2 ROS Generation

In PDT, the photosensitizers are transferred from the ground state into an excited state under a specific wavelength of the light source. The excited photosensitizers can react with molecular oxygen and generate cytotoxic ROS to induce oxidative damage or cell death [11]. We measured intracellular ROS generation by staining with DCFH-DA assay. As shown in Fig. 4.2, no obvious change can be found in ROS generation for the groups in the dark. When HT-29 cells were exposed to illumination (480 nm), there was a remarkable difference in ROS generation. ICN group could produce much more ROS (36.6%) than curcumin (3.39%). This result indicated that increasing intracellular ROS was induced by the photochemistry activation between laser and ICN, resulting in better therapeutic efficacy in killing cancerous cells.

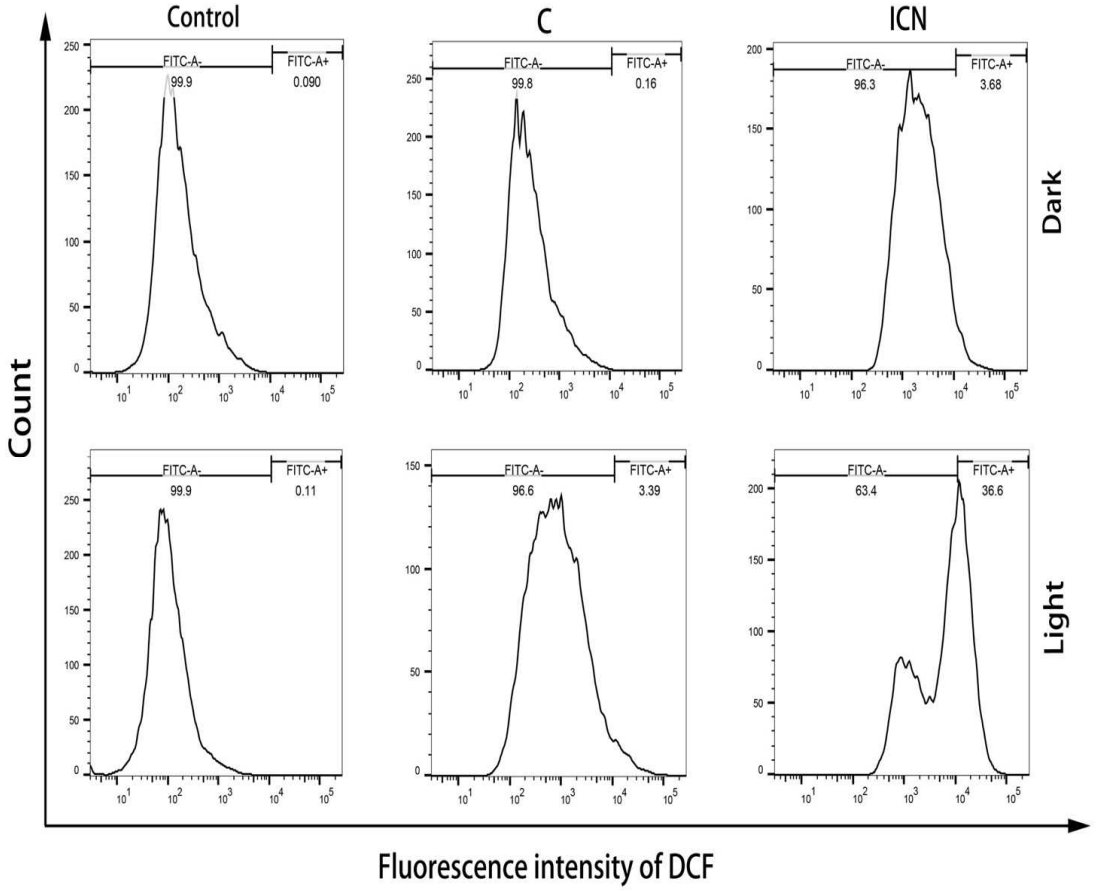

Figure 4. 2 Effect of curcumin/ ICN-photodynamic treatments on intracellular ROS generation in HT-29 cells. The cells were stained with DCFH-DA before flow-cytometric analysis.

4.3.3 Cellular Localization of Drugs

Among all cell organelles, mitochondria were frequently reported as the target site of singlet oxygen to improve the PDT efficacy [11]. The organelle mitochondria have been reported to be the most effective subcellular targets in PDT because ROS-induced mitochondrial DNA damage results in cytotoxicity in the PDT treatment [13]. Therefore, the desirable photosensitizers or their delivery carriers are usually expected to be accumulated within or stay close to mitochondria [14]. To verify the mitochondria-targeting capabilities of ICN, we investigated it by incubating the curcumin-treated HT-29 cells and ICN treated HT-29 cells. As shown in Figure 4.3, cells treated with ICN showed higher cellular uptake of ICN than curcumin in the mitochondria. This finding indicated that ICN was preferentially accumulated in mitochondria than curcumin, which demonstrated that ICN is a better photosensitizer than curcumin. To understand better about the specific targeting site in mitochondria, the images were filtered by a threshold as shown in Fig. 4.3 B (left column). After we merged the first row of Fig. 4.3 B (mitochondria images) with the second row of Fig. 4.3 B (drug images), we found that mitochondria were overlaid partially, and the overlaid part seems to be the bilayer membrane. This observation is very interesting and reasonable because the B cell family (Bcl- 2) members can regulate the release of signaling cell proteins from the space between the mitochondrial inner and outer membrane. [15] It was reported that caspase regulates the apoptosis when the cytochrome C activates cysteine specified proteases in the cytosol of mitochondria. [16]

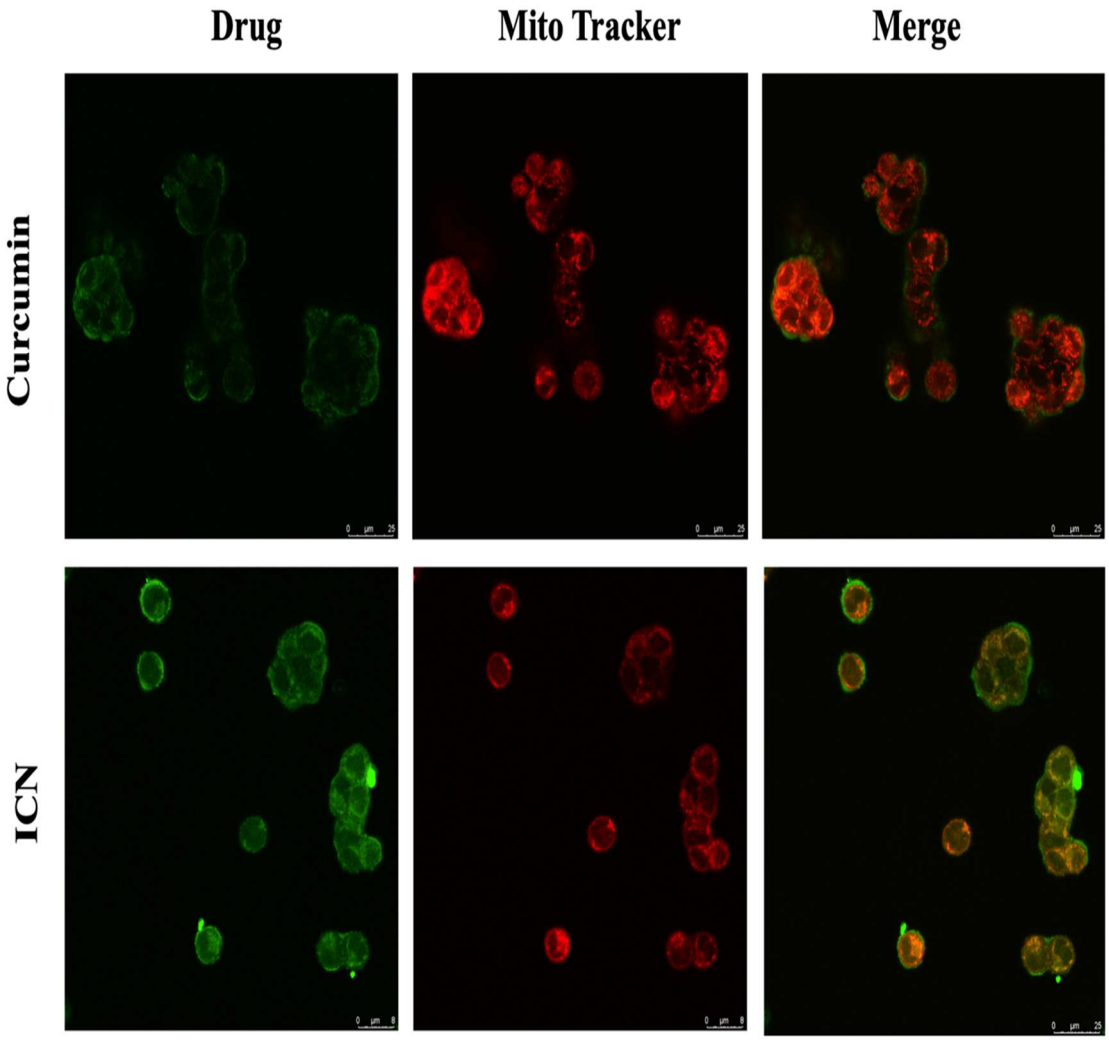

Figure 4. 3 A Confocal Laser scanning microscopy images of Cur and ICN (left column, green), and Mito-tracker Red (middle column, red) in HT-29 cell after incubation. Merged images (right column) of green and red channels refer to the co-localization levels of Cur and ICN with mitochondria. Scale bar is 25 µm.

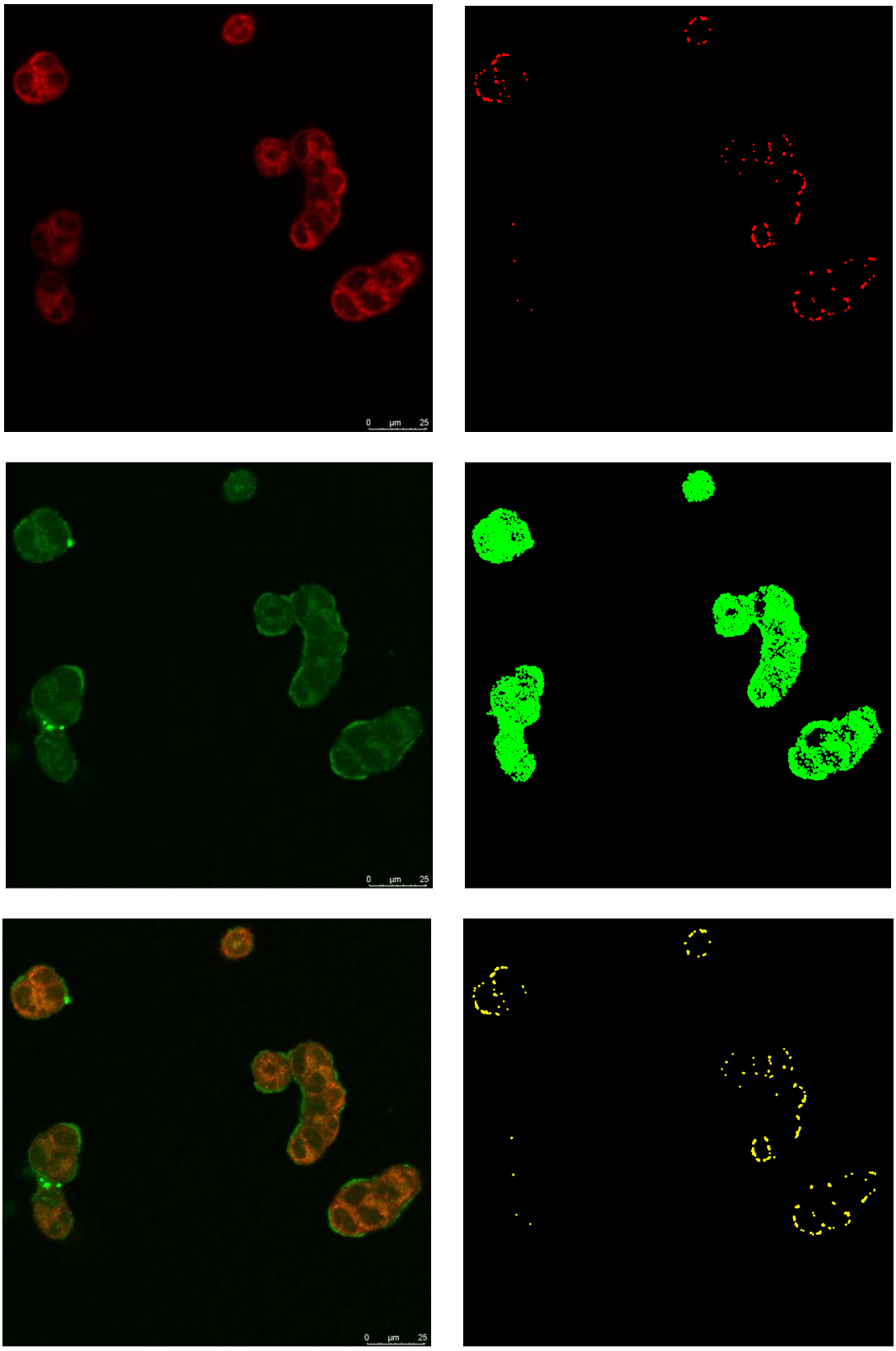
0 µm 25
0 µm 25
0 µm 25

Figure 4.3 B Confocal Laser scanning microscopy images of Cur and ICN (middle row, green), and Mito-tracker Red (top row, red) in HT-29 cell after incubation. Merged images (bottom row) of green and red channels refer to the co-localization levels of Cur and ICN with mitochondria. Raw images in left column and threshold images in right column.

4.3.4 Fluorescence-based Distribution under Different Environmental PHs

Fluorescence-based cellular uptake efficiency of ICN nanoparticles under environments with pH 6.7 and 7.5 was explored using HT-29 cells. As shown in Figure 4.4, the blank group where HT-29 cells alone under neutral conditions shows no fluorescence. For the ICN treated groups, cells under acidic environments (pH = 6.7) exhibit significantly stronger fluorescence than those in alkaline conditions (pH = 7.5), demonstrating a higher cellular uptake efficiency under acidic environments. The tumor microenvironment is known to be acidic due to reasons of glycolytic cancer cell metabolism and cell hypoxia [17,18]. The preferential accumulation in acidic might explain why ICN can largely improve cellular toxicity in the tumoral microenvironment.

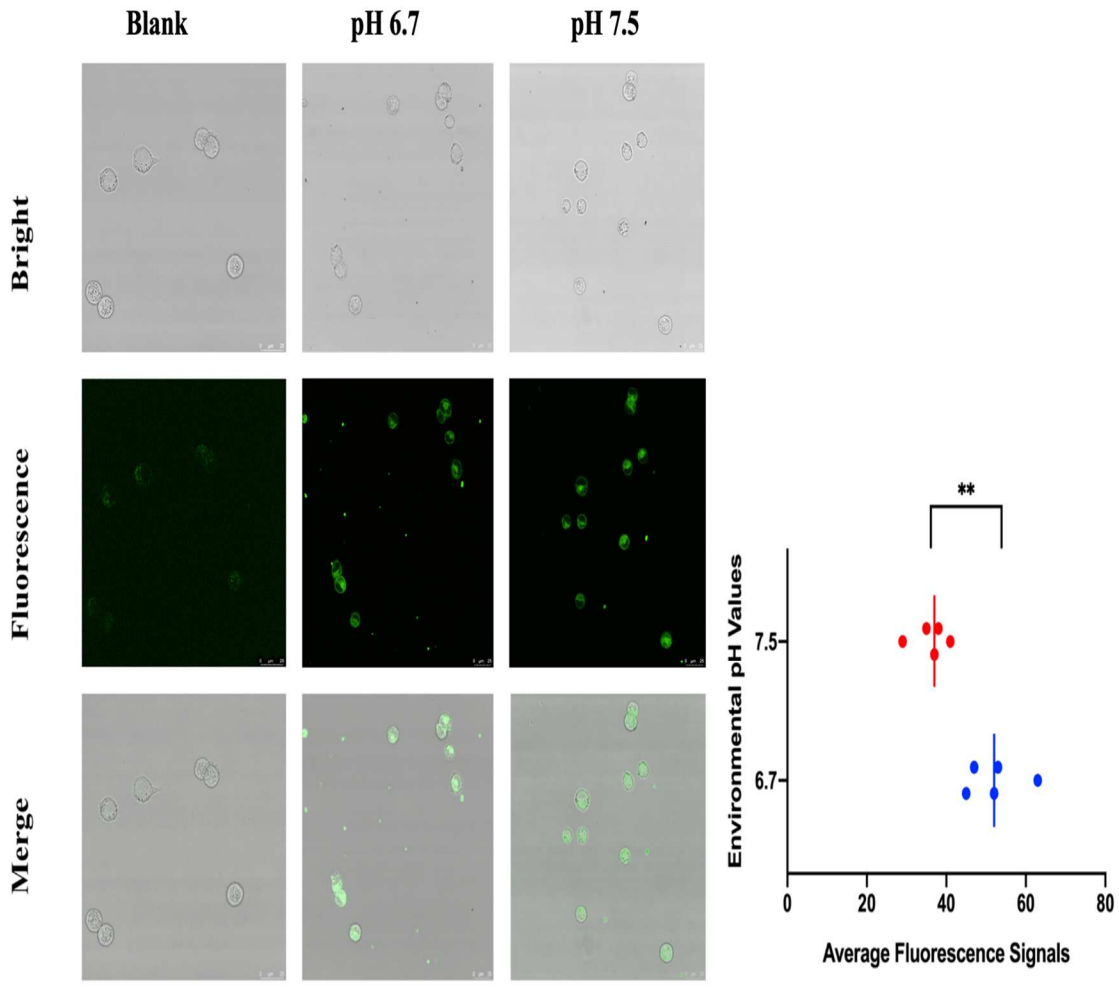

Figure 4. 4 Fluorescence-based cellular uptake efficiency under different pH environments. For the group adding ICN, cells under acidic environment (pH = 6.7) show stronger fluorescence than those under alkaline environments (pH = 7.5). The significant difference is observed between groups with different environmental pH values. (, $p < 0.01$)**

4.3.5 Apoptosis Analysis by Annexin V-FITC/PI Staining

The percentage of apoptotic HT-29 cells was assessed by Annexin V-fluorescein isothiocyanate (FITC) and propidium iodide (PI) double staining for flow cytometry analysis. High Annexin V and low PI staining (Q3) indicated the early apoptosis of cells. On the other hand, strong staining signals of both Annexin V label and PI (Q2) showed the cells were in the stage of necrosis or late apoptosis [19]. As shown in Figure 6, 8.2% of illuminated HT-29 cells were found to be apoptotic (early apoptosis added late apoptosis) when incubated with curcumin. However, after being treated with ICN, 41.16% (Q2 39.4%

and Q3 1.76%) of the total cells were induced to apoptosis. This assay indicates that ICN has a stronger anti-tumor effect in HT-29 cells compared with curcumin.

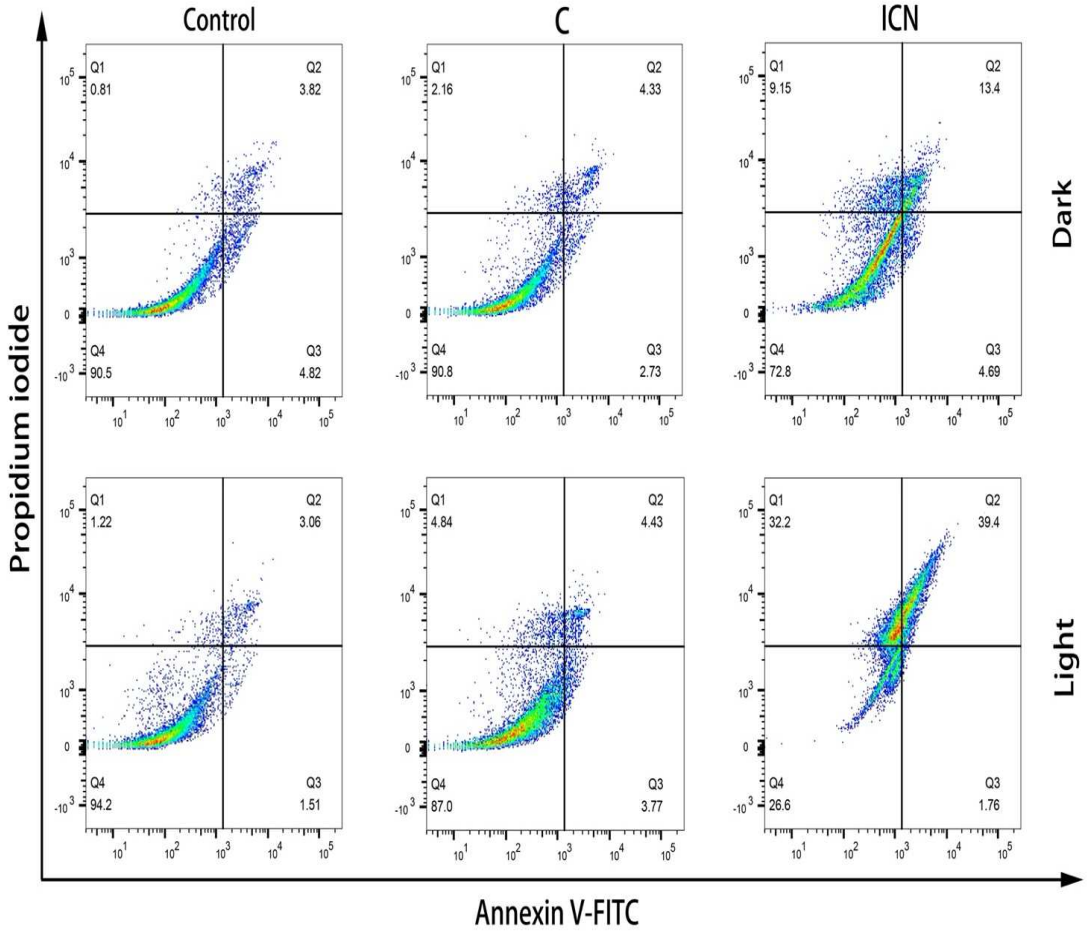

Figure 4. 5 Fluorescence-activated cell sorter profiles of Annexin V-FITC/PI staining of HT-29 cells undergoing apoptosis induced by curcumin and ICN in the dark or with irradiation.

3.6 In vivo Therapeutic Efficacy

We evaluated the in vivo anti-tumor therapeutic efficacy with in vivo mice model. [20] We randomly divided twelve tumor-bearing mice into three groups: PBS, ICN (without laser), and ICN (with laser). All mice were intravenously injected with either PSB or ICN with relatively equivalent tumor volume (~100 mm^3) and weight (20-24 g) at the dose of ICN 0.2μmol/kg to evaluate the anti-tumor efficacy. The medication was given every 3 days during a 15-day administration cycle. After the treatments, tumor volumes and body weights of each group were recorded, and the recorded results are plotted in Fig. 4.6 B for tumor volume and Fig. 4.6 D for mice body weight. Mice were sacrificed 7 days after

medication discontinuation. Tumors were excised out, photographed, and weighted as shown in Figs. 4.6 A and 4.6 C. The tumor volume (V) was calculated as V = (the major widths of the tumor × the minor widths of the tumor^2)/2. The tumor volume of the PBS injection or the control group increased continuously to a volume of 1660 mm^3 on day 21. For the group with ICN injection without laser irradiation, due to chemotherapy alone, the tumor volume also slightly shrank to 320 mm3 with a volume reduction of 80.7% compared with the control group. For the group with laser illumination and ICN drug injection, due to both chemotherapy and PDT, the tumor growth trend of the ICN- laser group declined significantly to 260 mm^3 with a tumor volume reduction of 84.3% compared with the control group. We found that the tumor volume was further reduced by 18.8% due to PDT by comparing the ICN + Laser group with the INC group, which demonstrates that PDT was a significant complementary treatment along with chemotherapy. The results also verified the enhanced anti-tumor effect of ICN by applying both chemotherapy and PDT treatments. Furthermore, in this study, the body weights of mice in each group were recorded and showed no significant changes in all mice during the whole experimental period as shown in Fig. 7D, which indicates the risks associated with the Irinotecan (diarrhea and weight loss) are negligible. To understand further about the therapeutic effects, hematoxylin and eosin (H&E) staining images of tumors and major organs were obtained after various treatments (Fig. 4.7). There were no obvious cell morphology abnormalities and cell damage found in the collected major organs. H&E-stained sections of colon cancer from ICN treated groups were found to damage tumor cell nuclei. These results demonstrated ICN/laser combination therapy was considered to be safe for cancer treatment.

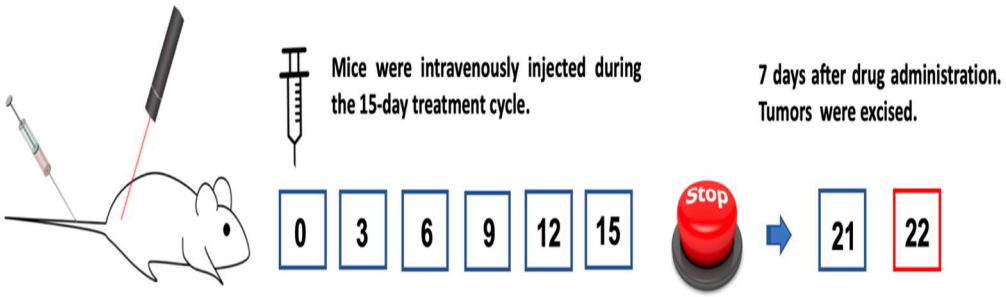

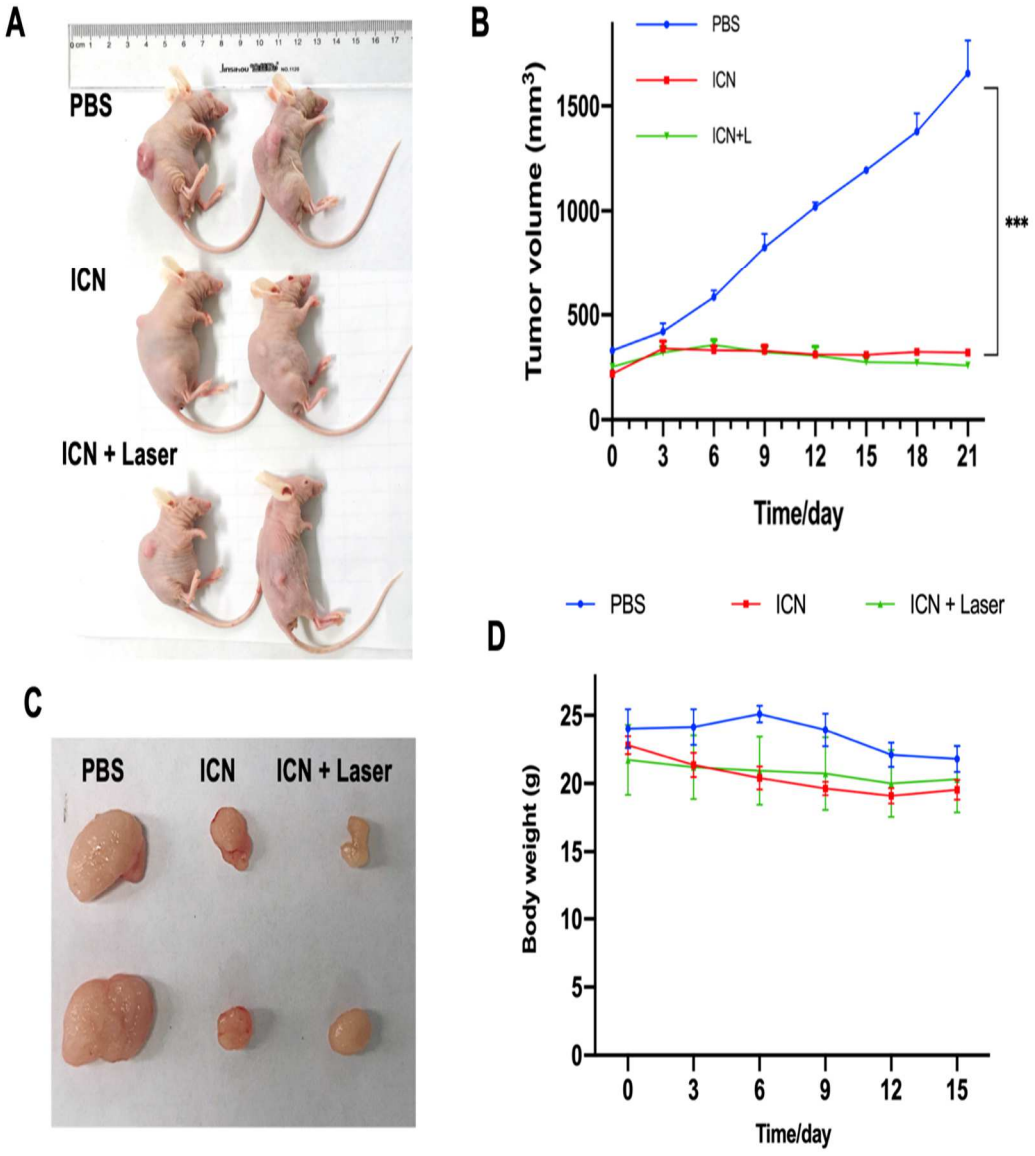

Figure 4. 6 . In vivo antitumor effects of HT-29 tumor-bearing mice were intravenously injected with ICN and PBS solutions. Tumors were excised out, photographed, and weighted (A) and (C). ICN+L groups were treated accompanied by illumination (80 mW /cm2). Compared with control, both ICN treated groups had antitumor effect and ICN + Laser group had the lowest tumor volume (B). Negligible changes of Body weight (D).

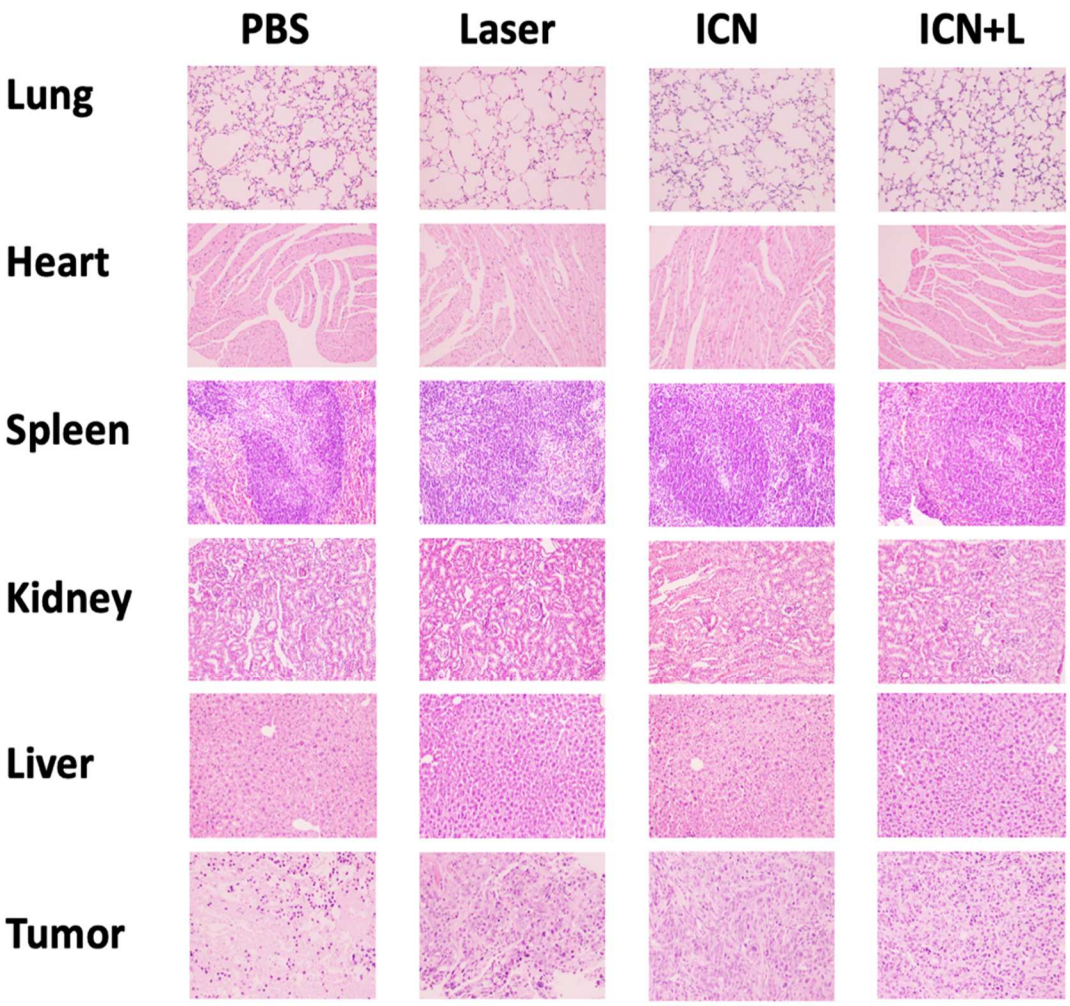
PBS
Laser
ICN
ICN+L
Lung
Heart
Spleen
Kidney
Liver
Tumor

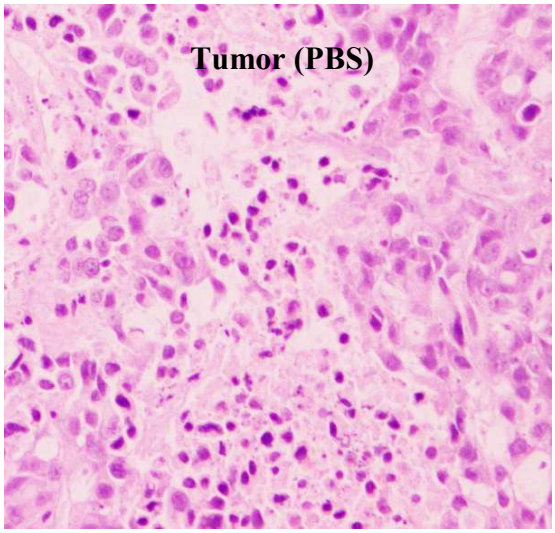
Tumor (PBS)

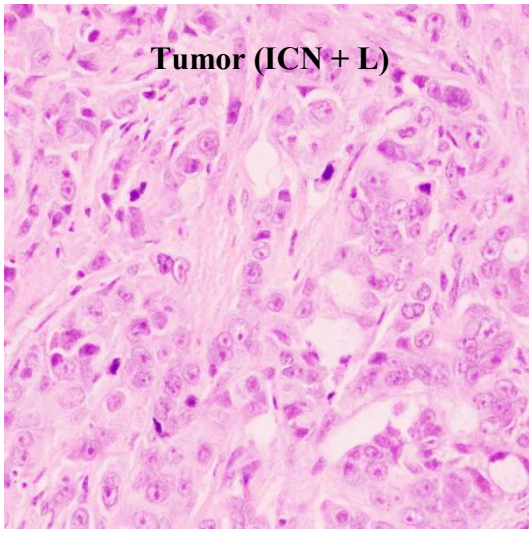
Tumor (ICN + L)

Figure 4. 7 Hematoxylin and eosin (H&E) staining images of the main organs from different groups of mice after receiving with various treatments.

4. Conclusions

In summary, irinotecan hydrochloride and curcumin can form as a carrier-free nanoparticle (ICN) through a straightforward self-assembly approach. This unique nanoparticle not only overcame the hydrophobicity of curcumin but also enhanced the anti-tumor efficacy of irinotecan by integrating multiple treatment modalities. In this study, we found that ICN, as both the chemotherapy agent and the PDT photosensitizer, could enhance the cancer cell treatment efficiency when exposed to the light source. We found that this anti-tumor effect was caused by higher cellular uptake efficiency under acidic tumor microenvironments and subsequent intracellular ROS formation in the presence of diode laser irradiation. Altogether, our results indicate the potential of using ICN in the combination of chemotherapy and photodynamic therapy with synergistic anti-tumor efficacy.

Reference

[1] R.L. Siegel, K.D. Miller, A. Jemal, Cancer statistics, 2019. CA A Cancer J Clin, 69 (2019) 7-34. https://doi.org/10.3322/caac.21551

[2] M. O. Palumbo, P. Kavan, W. H. Miller, L. Jr. Panasci, S. Assouline, N. Johnson, V. Cohen, F. Patenaude, M. Pollak, R. T. Jagoe, G. Batist, Systemic cancer therapy: achievements and challenges that lie ahead, Front Pharmacol. 4 (2013) 57, https://doi.org/10.3389/fphar.2013.00057

[3] S. H. Chen, G. Lahav, Two is better than one; toward a rational design of combinatorial therapy. Curr. Opin. Struct. Bio. 41 (2016) 145–150. https://doi.org/10.1016/j.sbi.2016.07.020

[4] R. Bayat Mokhtari, T. S. Homayouni, N. Baluch, E. Morgatskaya, S. Kumar, B. Das, H. Yeger, Combination therapy in combating cancer. Oncotarget. 23 (2017) 38022–38043. https://doi.org/10.18632/oncotarget.16723

[5] Y. Wen, W. Zhang, N. Gong, Y. F. Wang, H. B. Guo, W. Guo, P. C. Wang, X. J. Liang, Carrier-free, self-assembled pure drug nanorods composed of 10-hydroxycamptothecin and chlorin e6 for combinatorial chemo-photodynamic antitumor therapy in vivo, Nanoscale 38 (2017) 14347–14356. https://doi.org/10.1039/c7nr03129g

[6] K. Zheng, H. Liu, X. Liu, Y. Wang, L. Li, S. Li, J. Xue, M. Huang, M, Tumor Targeting Chemo- and Photodynamic Therapy Packaged in Albumin for Enhanced Anti-Tumor Efficacy, Int. J. Nanomedicine. 15 (2020) 151–167. https://doi.org/10.2147/IJN.S227144

[7] B. Shrestha, L. Tang, G. Romero, Nanoparticles□Mediated Combination Therapies for Cancer Treatment. Adv. Therap., 2 (2019)1900076. doi:10.1002/adtp.201900076

[8] D. van Straten, V. Mashayekhi, H. S. de Bruijn, S. Oliveira, D. J. Robinson, Oncologic Photodynamic Therapy: Basic Principles, Current Clinical Status and Future Directions, Cancers, 2 (2017) 19. https://doi.org/10.3390/cancers9020019

[9] A. P. Castano, T. N. Demidova, M. R. Hamblin, Mechanisms in photodynamic therapy: part one-photosensitizers, photochemistry and cellular localization, Photodiagnosis Photodyn Ther. 4 (2004) 279–293. https://doi.org/10.1016/S1572-1000(05)00007-4

[10] Y. Guo, S. Sheng, M. C. Lun, S-M. Tsai, W-C. Chin, R. Hoglund, C. Li, Photodynamic therapy excited by Cerenkov Radiation from Cesium-137 irradiator: in vitro studies, Clin. Onco. Res., 3 (2020) 6. https://doi.org/10.31487/j.COR.2020.06.07

[11] M. H. Schmidt, D. M. Bajic, K. W. Reichert, T. S. Martin, G. A. Meyer, H. T. Whelan, Light-emitting Diodes as a Light Source for Intraoperative Photodynamic Therapy, Neurosurgery, 3 (1996) 552–557. https://doi.org/10.1097/00006123-199603000-00025

[12] G. Pau, F. Fuchs, O. Sklyar, M. Boutro & W. Huber. EBImage--an R package for image processing with applications to cellular phenotypes. Bioinformatics. 26 (2010), 979–981. https://doi.org/10.1093/bioinformatics/btq046

[13] A. Amalraj, A. Pius, S. Gopi, Biological activities of curcuminoids, other biomolecules from turmeric and their derivatives - A review. J Tradit Complement Med. 2 (2016) 205-233. https://doi.org/10.1016/j.jtcme.2016.05.005

[14] B. S. S. Vetha, E. Kim, P. Oh, S. Kim, S. Lim, M-H. Sojn, H-J. Jeong, Curcumin Encapsulated Micellar Nanoplatform for Blue Light Emitting Diode Induced Apoptosis as a New Class of Cancer Therapy, Macromol. Res. 27 (2019) 1179–1184 https://doi.org/10.1007/s13233-019-7168-3

[15] X. Lin, Y. Fang, Z. Tao, X. Gao, T. Wang, M. Zhao, S. Wang, Y. Liu, Tumor-Microenvironment-Induced All-in-One Nanoplatform for Multimodal Imaging-Guided Chemical and Photothermal Therapy of Cancer, ACS Appl. Mater. Interfaces, 28 (2019) 25043–25053. https://doi.org/10.1021/acsami.9b07643

[16] D. Wlodkowic, W. Telford, J. Skommer, Z. Darzynkiewicz, Apoptosis and beyond: cytometry in studies of programmed cell death, Methods Cell Biol. 103 (2011) 55–98. https://doi.org/10.1016/B978-0-12-385493-3.00004-8

[17] S. Jiang, R. Zhu, X. He, J. Wang, M. Wang, Y. Qian, S. Wang, Enhanced photocytotoxicity of curcumin delivered by solid lipid nanoparticles. Int. J Nanomedicine, 12 (2016) 167–178. https://doi.org/10.2147/IJN.S123107

[18] C. Ren, J. Zhang, M. Chen, Z. Yang, Self-assembling small molecules for the detection of important analytes, Chem. Soc. Rev. 43 (2014) 7257-7266

[19] D. Wlodkowic, W. Telford, J. Skommer, Z. Darzynkiewicz, Apoptosis and beyond: cytometry in studies of programmed cell death, Methods Cell Biol. 103 (2011) 55–98. https://doi.org/10.1016/B978-0-12-385493-3.00004-8

[20] H. Xiao, Y. Guo, H. Liu, Y. Liu, Y. Wang, C. Li, J. Císař, D. Škoda, I. Kuřitka, L. Guo, V. Sedlařík, Structure-based design of charge-conversional drug self-delivery systems for better targeted cancer therapy, Biomaterials 232 (2020) 119701. https://doi.org/10.1016/j.biomaterials.2019.119701

CHAPTER 5

CONCLUSION AND DIRECTIONS FOR FUTURE WORKS

Based on the dissertation studies, combination therapy has provided the most effective results with regards to anti-cancer effects. It gained superiority from the ability to target multiple pathways, which is essential to minimize drug resistance because cancer cells are frequently incapable of adapting to the simultaneous toxic effects of two therapeutic agents [1]. Moreover, various pathways are dysregulated in cancer cells and have disrupted homeostatic environments that generally contribute to the rapid proliferation rate. For instance, studies have shown that various cancers have mutations in tumor suppressor genes, such as p53, that normally function to activate cell cycle arrest when DNA is damaged. [2] However, if tumor suppressor genes are mutated, accumulation of damaged DNA and inhibition of cell cycle arrest contribute to increasingly rapid proliferation rates and a more aggressive cancer [3]. Additionally, in cancer cells, data about therapeutic drugs and natural compounds inducing cancer cell demise remain to be clarified.

In the past decades, many advances have been made to benefit medicine and drug discovery, including genome wide association studies and Human Genome Project. [4] Based on the studies, huge amount of DNA variants has been found out to be associated with diseases. [5] Personal genomics have connection from genotypes to phenotypes and provide the data for the diseases. Personalized medicine (Figure 5.1) will be thus designed by combination of genetic phenotypes and drug responses, providing patients with specific treatments that are based on their genotypes. [6]

the key towards effective cancer therapy generally relies on a specific approach that will improve the efficacy of treatment for different types of cancer. Future combination trials will allow personalized medication of cancer treatment, by targeting cancer subtype characteristics in the time frequency and concentration dependent manners. Based on all reported findings on the potential modulation of pro-survival mechanisms by natural compounds, it appears that therapeutic outcome could also be achieved through the inhibition of multiple Bcl-2 (B-cell lymphoma 2) family members and by modulating the NF-κB signaling pathways. [7] Targeted generation of ROS by natural compounds could play an important role in this tailor-made anticancer approach. Natural compounds like Curcumin (Figure 5.2) induce the upregulation of Nrf2 expression and was reported suppresses the activity of carcinogens in a Nrf2-dependent manner [8]. Curcuminoids are linear diarylheptanoids that upregulate Nrf2 expression and induce Nrf2 translocation to the nucleus to elicit its antioxidant effects by stabilizing protein levels of Nrf2. In addition, curcuminoids upregulate glutathione levels which have been shown to reduce ROS levels and remove carcinogens, aiding in chemoprevention. [9] In the meantime, Curcuminoids have features such as the blue region absorption, the long-wavelength cation photo-polymerization, and minimal cell cytotoxicity to normal cells, which make curcumin an

ideal candidate as photosensitizers in PDT. [9] In Chapter 3 and Chapter 4, our studies showed that when the co-delivering with irinotecan, Curcuminoids exhibited dramatically enhanced lung and gallbladder targeting, can improve macrophage-clearance escape and better colorectal cancer treatment with eradication of life-threatening diarrhea, which brings great hope for better-targeted chemotherapy and clinical translation. [10] Various strategies based on combinatorial nanoparticles opened up many promising options toward addressing cancer drug resistance. Specific chemo-sensitizing agents, for instance, have been used in combination with chemotherapeutics to suppress MDR with defined mechanisms. In clinical cancer treatment, drugs with different modes of action can be combined in a precisely controlled manner to maximize therapeutic efficacy and to minimize the likelihood of drug resistance development. Enabling uniform and concurrent delivery of drug combinations, maintaining the synergistic drug ratios, and controlling drug exposure sequence are the major advantages of nanoparticle-based combination therapy over the traditional cocktail administration [11].While batch-to-batch inconsistency and manufacturability are among the key challenges in many combinatorial nanoparticles, we believe that ongoing efforts on the advancement of combinatorial nanoparticles will lead to the ideal combination therapy. Moreover, using the combination therapy approach is economically effective when one of the therapeutic agents is approved by FDA. With the FDA approval, overall costs of combination therapy research are then reduced. This increases the cost efficiency of therapy, thereby benefiting the medically underrepresented and underserved groups.

To further improve the anti-cancer efficacy of current combination therapy methods, it is better to combine immunotherapy with other therapies in my future work. This treatment can simulate immune system to fight against cancer or infections. Currently there are few types of immunotherapy methods including immune checkpoint inhibitors and T-cell transfer therapy [12]. PD-1/PD-L1 (programmed death) pathway and immunotherapy by blocking immune checkpoint proteins, the immune system can overcome cancer's ability to resist the immune responses and to stimulate the body's own mechanisms to defenses against cancer. [13] Adoptive T cell therapy has utilized engineered tumor-specific T cells that are infused into patient. In another type of T-cells therapy, T-cells are engineered express chimeric antigen receptors (CARs) to recognize cancer specific antigens.[14]

Compared to the combination of chemotherapy and photodynamic therapy methods in the dissertation, the inclusion of immunotherapy allows immune system to help patients in fighting cancers. The major organs associated with this type of therapy are the lymph system and thymus. In this dissertation, we used BALB/c nude mice for developing the xenografted tumor model. The nude gene mutated mice are showing the lack of fur on skin and abnormal thymus. This deficiency of thymus induced T-cells allows this type of mice to accept xenografts of malignancies. However, the dysfunction of T-cells leads it to an undesired animal model for immunotherapy. To address this issue, other strains of laboratory mice should be used for this future combination therapy studies like C57BL/6 mouse. (Fig. 5.3)

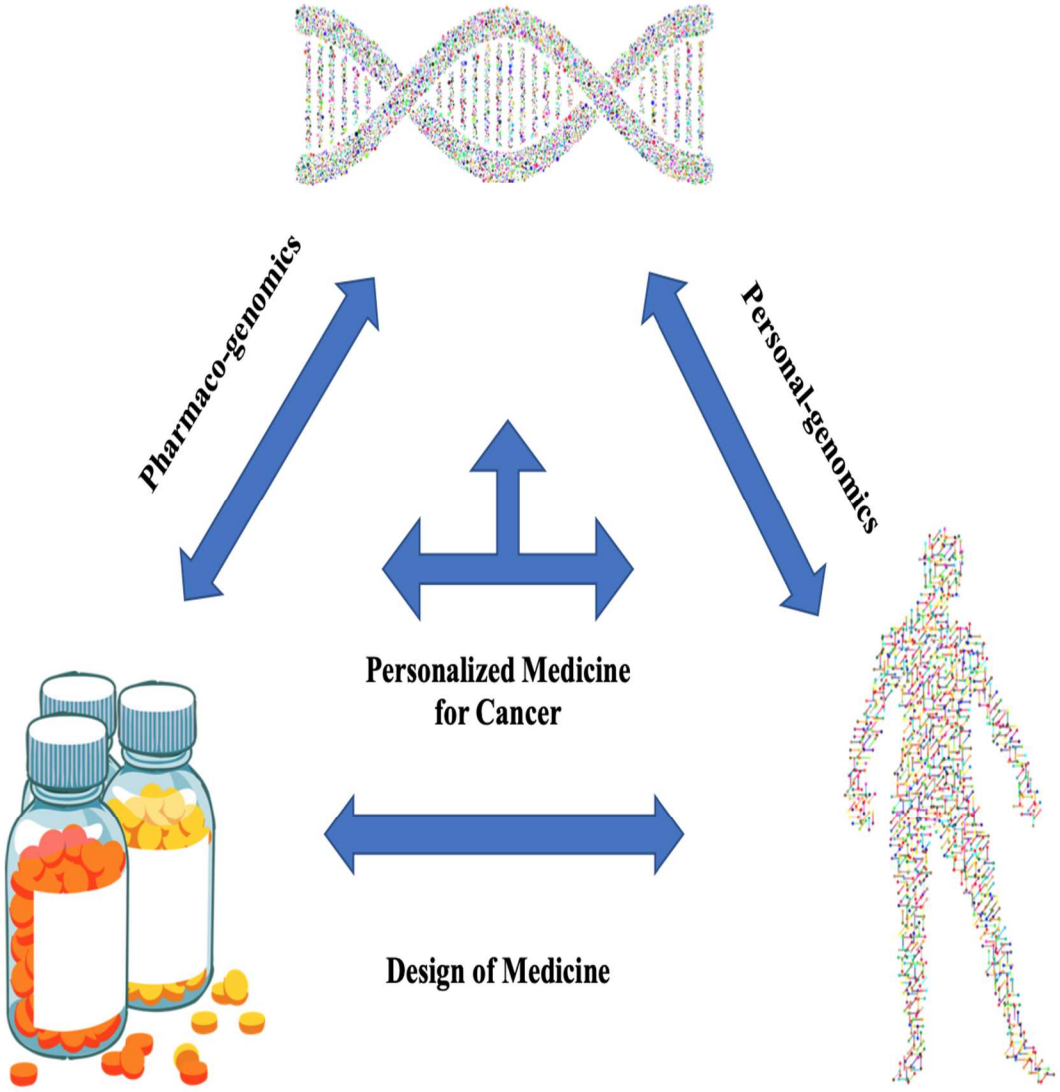

Figure 5. 1 Personalized medicine for cancer.

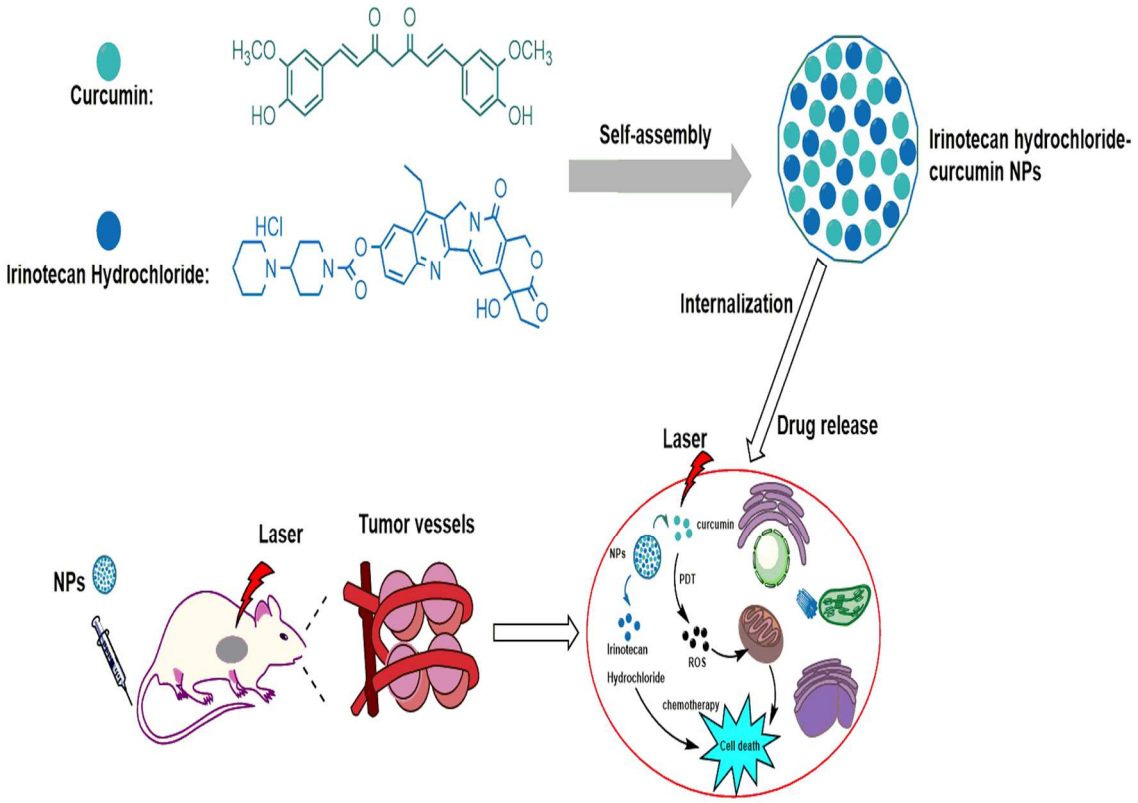

Figure 5. 2 Natural compounds: Curcumin for combination therapy.

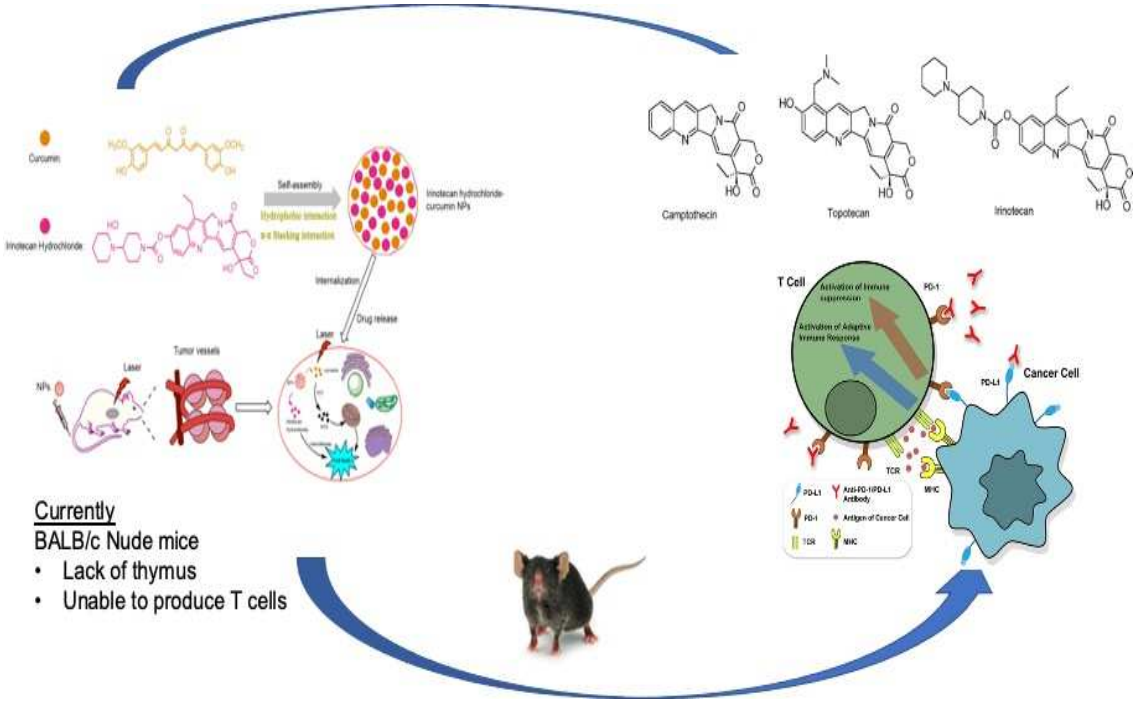

Figure 5.3 Immunotherapy involved combination therapy.

References

[1] Zimmermann GR, Lehar J, Keith CT. Multi-target therapeutics: when the whole is greater than the sum of the parts. Drug Discov Today. 12 (2007) 34-42.

[2] Muller PA, Vousden KH. p53 mutations in cancer. Nat Cell Biol. 15 (2013) 2-8.

[3] Marek L, Ware KE, Fritzsche A, Hercule P, Helton WR, Smith JE, McDermott LA, Coldren CD, Nemenoff RA, Merrick DT, Helfrich BA, Bunn PA Jr, Heasley LE. Fibroblast growth factor (FGF) and FGF receptor-mediated autocrine signaling in non-small-cell lung cancer cells. Mol Pharmacol. 75 (2009) 196-207.

[4] Collins, F S et al. Variations on a theme: cataloging human DNA sequence variation. 278 (1997) 1580-1581

[5] Hindorff, Lucia A et al. Potential etiologic and functional implications of genome-wide association loci for human diseases and traits. PNAS,106 (2009) 9362-9367.

[6] Overby CL, Tarczy-Hornoch P. Personalized medicine: challenges and opportunities for translational bioinformatics. Per Med. 10 (2013) 453-462

[7] Cotter FE. Unraveling biologic therapy for Bcl-2-expressing malignancies. Semin Oncol. 31 (2004) 18-21.

[8] Anagnostou VK, Lowery FJ, Zolota V, Tzelepi V, Gopinath A, Liceaga C, Panagopoulos N, Frangia K, Tanoue L, Boffa D, Gettinger S, Detterbeck F, Homer RJ, et al. High expression of BCL-2 predicts favorable outcome in non-small cell lung cancer patients with non-squamous histology. BMC Cancer. 10 (2001) 186.

[9] Das L, Vinayak M. Long term effect of curcumin in restoration of tumour suppressor p53 and phase-II antioxidant enzymes via activation of Nrf2 signalling and modulation of inflammation in prevention of cancer. PLoS One. 10 (2015) e0124000.

[10] Panahi Y SA, Beiraghdar F, Nouzari SMH, Jalalian HR, Sahebkar A. Antioxidant effects of bioavailability-enhanced curcuminoids in patients with solid tumors: A randomized double-blind placebo-controlled trial. Journal of Functional Foods. 6 (2014) 615-622.

[11] Bayat Mokhtari R, Homayouni TS, Baluch N, et al. Combination therapy in combating cancer. Oncotarget. 8 (2017) 38022-38043

[12] National Cancer Institute. About cancer. NIH. Cancer.gov

[13] Brahmer, Julie R et al. Safety and activity of anti-PD-L1 antibody in patients with advanced cancer. The New England journal of medicine vol. 366 (2012): 2455-65

[14] Ott, Patrick A et al. “Combination immunotherapy: a road map.” Journal for immunotherapy of cancer vol. 5 16. 21 Feb. 2017